Human immunodeficiency virus-1 induces host genomic R-loop and preferentially integrates its genome near the R-loop regions

Kiwon Park[1,2¶], Dohoon Lee[3,4¶], Jiseok Jeong[1,2], Sungwon Lee[1,2], Sun Kim[5], and Kwangseog Ahn[1,2,6*]

[1]Center for RNA Research, Institute for Basic Science, Seoul 08826, Republic of Korea

[2]School of Biological Sciences, Seoul National University, Seoul 08826, Republic of Korea

[3]Bioinformatics Institute, Seoul National University, Seoul 08826, Republic of Korea

[4]BK21 FOUR Intelligence Computing, Seoul National University, Seoul 08826, Republic of Korea

[5]Department of Computer Science and Engineering, Seoul National University, Seoul 08826, Republic of Korea

[6]SNU Institute for Virus Research, Seoul National University, Seoul 08826, Republic of Korea

*Corresponding author

Email: ksahn@snu.ac.kr (KA)

¶These authors contributed equally to this work.

Abstract

Although HIV-1 integration sites favor active transcription units in the human genome, high-resolution analysis of individual HIV-1 integration sites has shown that the virus can integrate into a variety of host genomic locations, including non-genic regions. The invisible infection by HIV-1 integrating into non-genic regions, challenging the traditional understanding of HIV-1 integration site selection, is more problematic because they are selected for preservation in the host genome during prolonged antiretroviral therapies. Here, we showed that HIV-1 integrates its viral genome into the vicinity of R-loops, a genomic structure composed of DNA–RNA hybrids. VSV-G-pseudotyped HIV-1 infection initiates the formation of R-loops in both genic and non-genic regions of the host genome and preferentially integrates into R-loop-rich regions. Using a HeLa cell model that can independently control transcriptional activity and R-loop formation, we demonstrated that the exogenous formation of R-loops directs HIV-1 integration-targeting sites. We also found that HIV-1 integrase proteins physically bind to the host genomic R-loops. These findings provide novel insights into the mechanisms underlying retroviral integration and the new strategies for antiretroviral therapy against HIV-1 latent infection.

Introduction

Retroviruses cause permanent host infections by integrating their reverse-transcribed viral genomes into the host genome. Retroviral integration considerably affects a wide range of biological phenomena, including the persistence of fatal human diseases and the shaping of metazoan evolution (*1*). Human immunodeficiency virus (HIV)-1 is a representative retrovirus underlying the global burden of acquired immune deficiency syndrome (AIDS) (*2*). The chromosomal landscape of HIV-1 integration has been shown to influence proviral gene expression, the persistence of integrated proviruses, and prognosis in antiretroviral therapy (*3-5*). Integration into the host genome is not random and displays distinct preferences for gene-dense regions, where active transcription occurs (*6*), by interacting with host factors, such as transcription activators, epigenetic marker binding proteins, and super enhancers (*7-13*). However, transcriptional activity is not the sole determinant of the HIV-1 integration site landscape (*10*). For instance, some highly expressed genes do not necessarily correspond to a high level of integration in PBMCs infected in culture with HIV (*14*). Despite their lower probability of integration, HIV-1 proviruses are observed in non-genic regions of the genomes of infected individuals (*4*). This indicates the possibility of there being an undiscovered mechanism or determinant that constitutes the correct genomic environment for HIV-1 integration.

An R-loop is a three-stranded nucleic acid structure that comprises a DNA–RNA hybrid and a displaced strand of DNA, and has long been considered a transcription byproduct (*15, 16*). R-loops in cellular genomes are enriched in actively transcribed genes as they occur naturally during transcription (*15, 17*). However, R-loop formation is not limited to gene body regions and is widespread in the genome (*15*). As a result of *in trans* R-loop formation,

57 R-loops are also abundant in non-genic regions, such as intergenic regions and repetitive
58 sequences, including transposable elements, centromeres, and telomeres (*15, 18-20*),
59 independent of the transcriptional activity of the genes harboring the R-loops. Although R-
60 loops have been identified as critical intermediates and regulators of a number of biological
61 processes (*15, 16, 21*), the dynamics and the role played by cellular R-loops in pathological
62 contexts remain unclear.

63 R-loops are important contributors to molding the genomic environment and spatial
64 organization of the cellular genome, and can potentially play a novel role in host-pathogen
65 interaction. In the cellular genome, R-loops relieve superhelical stresses and are often
66 associated with open chromatin marks and active enhancers (*22, 23*), which are also distributed
67 over HIV-1 integration sites (*6, 9, 10*). In transcription-induced R-loop formation, a guanine-
68 quadruplex (G4) structure can be generated in the non-template DNA strand of the R-loop (*24*).
69 A recent study showed that G4 DNA can influence both productive and latent HIV-1 integration
70 (*25*). In addition, R-loops are prevalent non-canonical B-form DNA structures (*26*) and
71 intermediates between the B-form DNA and A-form RNA conformations (*27*). It has recently
72 been reported that the B-to-A transition in the target DNA occur during retroviral integration
73 (*27, 28*). Accumulating evidence suggests that host genomic R-loops are undiscovered host
74 factors in the HIV-1 integration site selection mechanism that dynamically interact with the
75 host genomic environment.

76 Here, we showed a notable role for R-loops in the interaction between HIV-1 and its
77 host, specifically in HIV-1 integration. VSV-G-pseudotyped HIV-1-infection induces host
78 cellular R-loop formation, and the R-loop rich regions of the host genome are preferred for
79 HIV-1 integration in diverse cell types. HIV-1 integrase proteins showed considerable binding

affinity for nucleic acid substrates containing R-loop structures. Our results suggest that R-loops are important components of the host genomic environment for HIV-1 integration site determination.

Results

Host genomic R-loops accumulate by VSV-G-pseudotyped HIV-infection in diverse cell types

To investigate the relationship between HIV-1 infection and host cellular R-loops, we first analyzed R-loop dynamics in different types of cells infected with HIV-1 at early post-infection time points using DNA–RNA immunoprecipitation followed by cDNA conversion coupled with high-throughput sequencing (DRIPc-seq) using a DNA–RNA hybrid-specific binding antibody, anti-S9.6 (*29*). HeLa cells, primary $CD4^+$ T cells isolated from two individual donors, and the $CD4^+/CD8^-$ T cell lymphoma Jurkat cell line were infected with the VSV-G-pseudotyped HIV-1-EGFP in a time-course manner. The infected cells were harvested at the same post-seeding time point but at 0, 3, 6, and 12 h post infection (hpi) for DRIPc-seq library construction (Fig. 1A and S1A-C Fig.). Our DRIPc-seq analysis yielded loci-specific R-loop signals at the referenced R-loop-positive loci (RPL13A and CALM3) and an R-loop-negative locus (SNRPN) (*29*), which were both strand-specific and highly sensitive to pre-immunoprecipitation *in vitro* RNase H treatment in HeLa cells, $CD4^+$, and Jurkat T cells (Table S1-3). Notably, the number of DRIPc-seq peaks mapped to the human reference genome increased markedly during the early post infection with HIV-1 (3 and 6 hpi for HeLa cells and 6 and 12 hpi for $CD4^+$ and Jurkat T cells; Fig. 1B). Most of the peaks that mapped in cells harvested at 0 hpi were commonly found in all other samples, but a significant numbers of

103 unique peaks were observed after infection (Fig. 1C).

104 In addition to the DRIPc-seq data analysis, we used different biochemical approaches
105 to examine R-loop accumulation after HIV-1 infection in HeLa cells. R-loop accumulation in
106 HIV-1-infected cells was observed using DNA–RNA hybrid dot blots with the anti-S9.6
107 antibodies (Fig. 1D). Dot intensity significantly increased upon HIV-1 infection at 6 hpi and
108 the enhanced R-loop signals on the dot blots of HIV-1-infected cells were highly sensitive to
109 *in vitro* treatment with RNase H (Fig. 1D). This result is highly consistent with our DRIPc-seq
110 data analysis of HIV-1-infected HeLa cells. Subsequently, we observed HIV-1-induced R-loops
111 using an immunofluorescence assay by probing HIV-1-infected or non-infected control cells
112 with S9.6 antibody at 6 hpi (Fig. 1E). After subtracting the nucleolar signal, the nuclear
113 fluorescence signal associated with R-loops was significantly enhanced in cells infected with
114 HIV-1 (Fig. 1E). We validated and quantified HIV-1-infection induced R-loop formation on the
115 host genome in a genome-site-specific manner by using DRIP followed by real-time
116 polymerase chain reaction (DRIP-qPCR). In this experiment, the S9.6 signal was determined
117 for three and two HIV-1-induced-R-loop-positive (P1, P2, and P3) and -negative regions (N1
118 and N2), respectively, which were defined by DRIPc-seq data analysis (S2A-E Fig.). We
119 detected significantly increased R-loop signals that were highly sensitive to RNase H treatment
120 of pre-immunoprecipitates in the P1, P2, and P3 regions of HIV-1-infected cells at 6 hpi
121 compared to those in the cells harvested at 0 hpi (S3A Fig.). However, the HIV-1-induced R-
122 loop-negative regions N1 and N2, did not show significant R-loop accumulations (S3A Fig.).

123 Importantly, the R-loop signal was enriched even in cells infected with HIV-1 when
124 the reverse transcription or integration of HIV-1 was blocked by enzyme inhibitors, such as
125 nevirapine (NVP) or raltegravir (RAL) (S3B and S3C Fig.). This result indicates that the

126 enrichment of R-loop signals in cells originates from the host genome, but not from DNA-RNA
127 hybrid formation during the viral life cycle or transcriptional burst from integrated HIV-1
128 proviruses. In addition, we confirmed that nearly 100% of DRIPc-seq reads from HIV-1-
129 infected HeLa, $CD4^+$, and Jurkat T cells were aligned to the host cellular genome, but not to
130 that of HIV-1 (S3D Fig.). Together, these data demonstrated that HIV-1 infection induce host
131 genomic R-loop enrichment at early post-infection. This also suggests that HIV-1 infection
132 regulates R-loop dynamics in host cells, possibly by inducing either new R-loop formation or
133 stabilizing existing R-loops in the host cellular genome.

134

135 **R-loops accumulation after HIV-1 infection are widely distributed in both genic and non-**
136 **genic regions**

137 To investigate the distribution of cellular genomic R-loops during HIV-1 infection, we
138 conducted a genome-wide analysis of the DRIPc-seq data. Unique DRIPc-seq peaks observed
139 after HIV-1 infection were numerous and relatively long (Fig. 2A). This suggests that the R-
140 loops induced by HIV-1 infection occupy a genomic region larger than that of the R-loops
141 without HIV-1 infection. We observed a significant accumulation of R-loops over diverse
142 genomic compartments at the hpi of HIV-1-infection induced R-loop formation (Fig. 2B). The
143 presence of R-loops is often correlated with high transcriptional activity, and we found a
144 significantly high proportion of DRIPc-seq peaks enrichment upon HIV-1 infection in the gene
145 body regions (Fig. 2B). However, we also observed enrichment of HIV-1-infection induced
146 DRIPc-seq peaks proportions mapped to intergenic or repeat regions, including short
147 interspersed nuclear elements (SINEs), long interspersed nuclear elements (LINEs), and long
148 terminal repeat (LTR) retrotransposons, where transcription is typically repressed (Fig. 2B). In

149 addition, the proportion of DRIPc-seq peaks mapped to various genomic compartments
150 remained consistent over the hours following HIV-1 infection (Fig. 2C). This suggests that
151 HIV-1 infection does not induce R-loop enrichment at specific genomic features, but that R-
152 loops accumulation after HIV-1 infection is widely distributed. Although the expression of
153 repetitive elements is mostly repressed during normal cellular activities, HIV-1 infection could
154 activate endogenous retroviral promoters (*30, 31*). To investigate whether R-loop induction in
155 gene-silent regions is associated with transcriptome changes during HIV-1 infection, we
156 performed RNA sequencing (RNA-seq) of HIV-1-infected HeLa cells at 0, 3, 6, and 12 hpi.
157 Consistent with previous reports, we observed an increase in the expression levels of repetitive
158 elements at later time points post-infection (S4A Fig. 12 hpi). In contrast, we found that the
159 expression levels of SINEs, LINEs, and LTRs were even lower at both 3 and 6 hpi compared
160 with those at 0 hpi whereas HIV-1-induced R-loops were significantly accumulated compared
161 with those at 0 hpi (S4A Fig.). We further examined the expression profiles of genes containing
162 the R-loop in HeLa cells. The expression profile of genes harboring HIV-1-induced R-loops in
163 their gene bodies showed very weak correlations with the signals of DRIPc-seq peaks at 3 hpi
164 (Pearson's $r = 0.21$, $P = 1.08 \times 10^{-84}$; Fig. 2D) and at 6 hpi (Pearson's $r = -0.34$, $P = 2.40 \times 10^{-}$
165 ^{228}; Fig. 2D), which implies that the unique R-loop peaks upon HIV-1 infection do not engage
166 in a transcriptional burst. In agreement with our DRIPc-seq and global RNA-seq data analysis,
167 the expression level of the genes harboring HIV-1-infection induced R-loops, which were
168 quantified by DRIP-qPCR (S3A Fig.), were not significantly affected by HIV-1 infection (S4B
169 Fig. and Table S4). Together, our data demonstrate that host cellular R-loop accumulation upon
170 HIV-1 infection is widely distributed in both genic and non-genic regions and is not necessarily
171 correlate with the expression levels of the genes harboring the R-loops.

172

173 **HIV-1 integration sites are enriched at systemically induced sequence-specific R-loop**
174 **regions in cell model**

175 HIV-1 infection is completed by integrating the viral genome into the host's through
176 dynamic interactions with the host genome (*32*). In addition, as HIV-1 infection induces R-
177 loop accumulation at early post infection hours, when the HIV-1 genome are imported into the
178 nucleus and integration may initiate (*33-35*), we hypothesized that host genomic R-loops play
179 a role in HIV-1 integration and possibly in integration site selection. To systemically and
180 directly assess the relationship between host genomic R-loops and HIV-1 integration in a
181 genome site-specific manner, we adapted and modified an elegantly designed episomal system
182 that induces sequence-specific R-loops through DOX-inducible promoters (*17*). To most
183 closely mimic the presence of the R-loop in the host cellular genome, we subcloned the R-
184 loop-forming portion of the mouse gene encoding AIRN (mAIRN) (*18*) or the non-R-loop-
185 forming ECFP sequence (*17*) with a DOX-inducible promoter into the piggyBac transposon
186 vector and co-expressed piggyBac transposase in HeLa cells. The mAIRN gene sequence
187 possesses a high GC skew that causes R-loop structure formation upon transcription by
188 hybridizing newly synthesized RNA back to the template DNA strand, and the non-template
189 DNA strand to remains looped out in a single-stranded form (*18, 36*). In contrast, the ECFP
190 sequence possesses a low GC skew that does not form a stable R-loop at the site of transcription.
191 Thus, it was used as an R-loop-forming negative sequence. These R-loop forming (mAIRN) or
192 non-R-loop forming (ECFP) sequences are nonhuman sequences. Therefore, our cell model
193 allowed us to induce and quantify R-loop formation at designated genomic regions and
194 distinguish R-loop formation from endogenous R-loops on the cellular genome, which are not
195 sequence-specific and impossible to control for induction. Moreover, using this system we can
196 quantify R-loop-associated site-specific HIV-1 integration events at designated regions, which

197 can also be distinguished from HIV-1 integration events at endogenous host genomic loci. We
198 designated the pool of cells with the R-loop forming sequence (mAIRN) inserted into its
199 genome as "pgR-rich (piggyBac R-loop rich)" cell line and the pool of cells with the non-R-
200 loop forming sequence (ECFP) inserted into its genome as "pgR-poor (piggyBac R-loop poor)"
201 cell line (Fig. 3A).

202 A similar number of the copies of the piggyBac transposon were successfully delivered
203 to the genome of each cell line (S5A Fig.) and DOX treatment strongly induced the
204 transcriptional activity of mAIRN or ECFP without affecting the transcription of endogenous
205 loci in either cell line (S5B and S5C Fig.). Although the transcription of mAIRN or ECFP was
206 strongly induced by DOX treatment, the activity did not exceed that of the endogenous loci in
207 either cell line (S5D and S5E Fig.). Although the two cell lines showed comparable levels of
208 DOX-inducible transcriptional activity at the designated sequences (Fig. 3B), only the pgR-
209 rich cells exhibited robust RNase H-sensitive stable R-loop formation upon DOX treatment
210 (Fig. 3C, mAIRN). In contrast, R-loops were weakly formed in the pgR-poor cells where a
211 non-R-loop-forming sequence (ECFP) was inserted into the genome (Fig. 3C, ECFP).

212 To examine whether the formation of 'extra' R-loops in the host genome influence
213 HIV-1-infection in host cells, we infected both cell lines with VSV-G-pseudotyped HIV-1-
214 luciferase viruses and examined the luciferase activity. Notably, we found that pgR-rich cells
215 showed significantly higher luciferase activity only when R-loops were induced by DOX
216 treatment, whereas pgR-poor cells showed comparable luciferase activity regardless of
217 transcriptional activation by DOX treatment (Fig. 3D). We sequenced HIV-1 integration sites
218 in HIV-1-infected pgR-poor and pgR-rich cells to directly quantify site-specific integration
219 events in sequence-specific R-loop regions. Remarkably, integration events were significantly

220 higher in pgR-rich cells only when R-loops were induced by DOX treatment (Fig. 3E).
221 However, the number of HIV-1 integration-seq mapped reads within the non-R-loop forming
222 sequence in pgR-poor cells remained very low, even after transcriptional activation by DOX
223 treatment (Fig. 3E). HIV-1 integration was enriched in the vicinity of R-loop forming regions
224 in the pgR-rich cell line upon DOX treatment, but the enrichment was not observed in pgR-
225 poor cells that did not form stable R-loops, even after transcriptional activation by DOX
226 treatment (Figs. 3F and 3G). This cell-based R-loop-inducing system with independent control
227 over transcription and R-loop formation enabled the direct measurement of HIV-1 integration
228 events at defined R-loop regions. The results indicated that host genomic R-loops are preferred
229 by HIV-1 integration. Moreover, our data suggest that transcriptional activity itself is not
230 sufficient for HIV-1 integration site determination, but that the formation of R-loops accounts
231 for HIV-1 integration site selection.

232

233 **Host genomic R-loop regions are frequently targeted by HIV-1 integration**

234 We attempted to further validate the relationship between R-loops and HIV-1
235 integration site selection by global analysis of HIV-1 integration sites in the endogenous
236 genomic regions of HIV-1 infected host cells. We performed HIV-1 integration site sequencing
237 in HIV-1 infected HeLa cells, $CD4^+$, and Jurkat T cells, and analyzed the sequencing data
238 combined with our DRIPc-seq data. We counted and compared the number of successfully
239 integrated proviruses in the R-loop regions (the combined genomic regions within 30-kb
240 windows centered on DRIPc-seq peaks from 0, 3, 6, and 12 hpi) to those in non-R-loop-forming
241 regions (the total genomic regions outside of the 30-kb windows centered on DRIPc-seq peaks).
242 Notably, we detected approximately three to four times more integration in the R-loop regions

243 than in other genomic regions without R-loops in HeLa cells, $CD4^+$, and Jurkat T cells (Fig.
244 4A). Notably, HIV-1 integration sites preferred the centeral and nearby areas of the R-loops
245 regions (Fig. 4B). We observed biases in HIV-1 integration in HIV-1-induced R-loop-positive
246 regions, P1-P3, where showed highly induced R-loop signals upon HIV-1 infection in DRIPc-
247 seq analysis and DRIP-qPCR (Fig. 4C). In contrast, HIV-1 integration sites were not detected
248 in the R-loop-negative regions N1 and N2 (Fig. 4D). Overall, our results from bioinformatics
249 analysis using different types of naïve host cells infected with HIV-1 are consistent with the
250 idea that the virus has a preference for targeting R-loop-forming regions for integration (Fig.
251 3), suggesting that R-loops are an important component of the host genomic environment for
252 HIV-1 integration site determination.

253

254 **HIV-1 integrase proteins physically interacts with R-loops on the host genome**

255 The HIV-1 intasome is tethered to the host genome for viral cDNA integration.
256 Intasomes consist of HIV-1 viral cDNA and the HIV-1 integrase proteins. We observed that
257 HIV-1 was preferentially integrated into the R-loops regions in the host genome; thus, we
258 hypothesized that the HIV-1 integrase protein could directly bind and be recruited to the
259 genomic R-loops. To test this hypothesis, we investigated whether HIV-1 integrase proteins
260 have a physical binding affinity for nucleic acid substrates with an R-loop structure. Although
261 HIV-1 integrases are DNA and RNA binding proteins (*37, 38*), their ability to bind to a three-
262 stranded nucleic acid structure that is composed of a DNA-RNA hybrid like R-loop has not
263 been investigated. We carried out an *in vitro* protein-nucleic acid binding assay by
264 electrophoretic mobility shift assay (EMSA) with Sso7d-tagged HIV-1 integrase (E152Q)
265 recombinant proteins and diverse structures of nucleic acid substrates including R-loops and
266 simple dsDNA duplexes. In this experiment, we used HIV-1 integrase protein with an active

site amino acid substitution, E152Q, to prevent any undesirable alternation in nucleic acid substrates by enzymatic activities of integrase proteins, such as 3'-processing. Notably, nucleic acid substrate consisted of an R-loop structure bound to HIV-1 integrase proteins with higher binding affinity than that of the simple dsDNA duplex (Fig. 5A). Additionally, the R-loop composing forms of nucleic acid structures, such as RNA-DNA hybrid with exposed ssDNA (R:D+ssDNA) and RNA-DNA hybrid (hybrid), also showed high binding affinity to integrases (S6A Fig. and Fig. 5A).

We validated the interaction between cellular genomic R-loops and HIV-1 integrase proteins by DNA–RNA hybrid immunoprecipitation using S9.6 antibodies against FLAG-tagged HIV-1 integrase-expressing HeLa cells (Fig. 5B). Under our experimental conditions, R-loops were reproducibly immunoprecipitated (S6B Fig.) and HIV-1 integrase proteins co-immunoprecipitated with the R-loops (Fig. 5C). DNA–RNA hybrids also co-immunoprecipitated with the positive control H3 (*39*) but not with the negative controls LaminA/C and Actin (*39*) (Fig. 5C). To verify the specificity of our co-immunoprecipitation results for R-loops and HIV-1 integrases, we performed DNA–RNA hybrid immunoprecipitation with RNase H treatment (S6C Fig.). The S9.6 signal of the immunoprecipitated nucleic acids was highly sensitive to RNase H treatment of the pre-immunoprecipitates (Fig. 5D). Accordingly, the blotting signal of the co-immunoprecipitated HIV-1 integrase and H3 proteins was significantly reduced upon RNase H treatment (Fig. 5E). We performed reciprocal immunoprecipitation using an anti-FLAG monoclonal antibody and detected the immunoprecipitated R-loops using dot blot analysis with anti-S9.6. R-loops, which were immunoprecipitated using HIV-1 integrase, and the S9.6 signal of immunoprecipitated nucleic acids was highly sensitive to RNase H treatment (Fig. 5F and S6D Fig.). Subsequently, we examined the interaction between the R-loops and HIV-1 integrase using a proximity-

291 ligation assay (PLA) in HIV-1-infected cells. We used two antibodies: one that binds to the
292 R-loops (anti-S9.6) and another that binds to GFP-tagged HIV-1 integrase. We detected PLA
293 signals in cells infected with HIV-IN-EGFP virions (*34*) and non-infected control cells. PLA
294 signals in non-infected cells were comparable to those in S9.6-alone and GFP-alone single
295 antibody-negative controls; however, PLA signals significantly increased upon HIV-1 infection
296 (Fig. 5G and S6E Fig.). Our data suggest that the HIV-1 frequently targets R-loop-rich regions
297 for viral genome integration by physically binding of HIV-1 integrase proteins to R-loop
298 structures on the host genome.

299

300

301 ## Discussion

302 In this study, we found that HIV-1 preferentially integrated into regions rich in R-loops,
303 suggesting that R-loops are novel host factors that contribute to HIV-1 integration site selection.
304 In our bioinformatics analysis, host cellular R-loops were induced by VSV-G-pseudotyped
305 HIV-1 infection and widespread in host genomic regions. Using our R-loop-inducible cell
306 models, R-loop formation, and not necessarily the transcriptional activity itself, was found to
307 be important for HIV-1 integration site determination. In addition, HIV-1 integrase proteins
308 favor physical binding with R-loops *in vitro*, and interact with host genomic R-loops in HIV-
309 1-infected cells. These results demonstrate that HIV-1 exploits and frequently targets the host
310 genomic R-loop regions for successful integration and infection.

311 One possible explanation for why HIV-1 integration shows a preference for host
312 genomic R-loop regions is that the R-loop structure may drive dynamics in the genomic
313 environment and the spatial organization of the genome, resulting in increased accessibility of
314 HIV-1 intasome binding to the target host genomic region. The R-loops display enhancer and
315 insulator chromatin states, that can act as distal regulatory elements by recruiting diverse
316 chromatin binding factors (*22*). This not only allows R-loops to drive dynamics in the genome,
317 but also possibly drives R-loop-mediated integration over long-range genomic regions. R-loop
318 regions exhibit increased chromatin accessibility. In the cellular genome, these structures
319 relieve superhelical stresses and are often associated with open chromatin marks and active
320 enhancers (*22, 23*), which are also distributed over HIV-1 integration sites (*6*). In the case of
321 transcription-induced R-loop formation, a guanine-quadruplex (G4) structure can be generated
322 in the non-template DNA strand of the R-loop, which is another contributor to genome
323 architecture (*24*). A recent study showed that G4 DNA can influence both productive and latent
324 HIV-1 integration, as well as the potential for reactivation of latent proviruses (*25*).

325 Another possible explanation for the preference of HIV-1 integration for host genomic
326 R-loops is that R-loops may play a collaborative role with host factors governing the HIV-1
327 integration site selection. Cellular R-loops are recognized and regulated by numerous cellular
328 proteins (*39, 40*). LEDGF/p75 (*9, 13, 41*) and CPSF6 (*7, 9*) are two decisive host factors that
329 direct HIV-1 integration by interacting with integrase or trafficking the viral preintegration
330 complex towards the nuclear interior (*7, 9*). In fact, these host factors have recently been
331 identified as potential R-loop-binding proteins in DNA–RNA interactome analysis (*39*) and R-
332 loop proximity proteomics (*40*), respectively. R-loops are tightly regulated by DNA damage
333 response proteins (*42*) and the DNA repair machinery plays an important role in HIV-1
334 integration process (*32*). For example, the Fanconi anemia pathway (*43, 44*), a well-known R-
335 loop regulatory pathway, has been recently proposed as an HIV-1 integration regulatory factor
336 exploited by HIV-1 (*45*). Considering theses previous studies and our current findings, we
337 propose R-loops as another putative host factor driving HIV-1 integration site determination,
338 and a possible intermediate regulator of HIV-1 integration site selection by such host proteins.

339 Our data showed that HIV-1 integrase proteins physically interacted with genomic R-
340 loops *in vitro* and in cells. Recent advancements in cryogenic electron microscopy (cryo-EM)
341 technology have revealed the conformational characteristics of the target DNA during retroviral
342 integration (*27, 28*). During retroviral integration, the target DNA undergoes a transition of its
343 conformation from B-form to A-form. R-loops, which represent intermediates between the B-
344 form DNA and A-form RNA conformations (*27*), may have an intrinsic preferential binding
345 ability to retroviral intasomes over other nucleic acid structures.

346

347

348 Viruses often take advantage of various host factors, and targeting the viral
349 components that manipulate the host cellular environment can be an effective strategy for
350 antiviral therapy. Our study showed the host genomic R-loops significantly accumulate shortly
351 after HIV-1 infection. Thus, it is possible that virion-associated HIV-1 proteins are responsible
352 for inducing these R-loops. For instance, the HIV-1 accessory protein Vpr causes genomic
353 damage (*46*) and transcriptomic changes during the early stages post infection(*47*), both of
354 which can lead to *in cis* and *in trans* R-loop formation (*16*). Another HIV-1 accessory protein,
355 Vif, counteracts the host antiviral factor, APOBEC3 (*48, 49*), which was recently found to
356 regulates cellular R-loop levels (*50*). Identifying the HIV-1 components responsible for
357 inducing host cellular R-loops, elucidating the mechanism by which they induce genome-wide
358 R-loop formation, and contributing to successful viral integration into selective genomic
359 regions, are areas for further research.

360 Although most HIV-1 integration occurs in genic regions (*4, 6*), HIV-1 proviruses are
361 also found in non-genic regions (*51*) and understanding these "transcriptionally silent"
362 proviruses is critical for developing strategies to completely eliminate HIV-1. In HIV-1 elite
363 controllers, who suppress viral gene expression to undetectable levels, HIV-1 proviruses in
364 heterochromatic regions are not eliminated but selected by the immune system (*5*). Moreover,
365 proviruses with lower expression level can persist in the host genome even during antiretroviral
366 therapy (*4*). However, the mechanism by which HIV-1 targets gene-silent regions for
367 "invisible" integration remains unclear. Our study has revealed that R-loops are enriched in
368 both genic and non-genic regions during HIV-1 infection, and that the virus preferentially
369 targets these R-loops for integration. We propose that R-loops, particularly those enriched in
370 non-genic regions, may represent the mechanism by which the virus achieves "invisible" and
371 permanent infection.

372 # Materials and methods

373 ## Cell culture

374 HeLa and HEK293T cells were cultured in Dulbecco's modified Eagle's medium (Gibco)
375 supplemented with 10% (v/v) fetal bovine serum (FBS, Cytiva), antibiotic mixture (100
376 units/ml penicillin–streptomycin, Gibco), and 1% (v/v) GlutaMAX-I (Gibco). Jurkat cells were
377 cultured in Roswell Park Memorial Institute (RPMI) 1640 medium (ATCC) supplemented with
378 10% (v/v) FBS (Cytiva). Cells were incubated at 37°C and 5% CO_2.

379 ## Virus production and infection

380 VSV-G-pseudotyped HIV-1 virus stocks were prepared by performing standard
381 polyethylenimine-mediated transfection of HEK293T monolayers with pNL4-3 ΔEnv EGFP
382 (NIH AIDS Reagent Program 11100) or pNL4-3. Luc.R-E (NIH AIDS Reagent Program, 3418)
383 along with pVSV-G at a ratio of 5:1. HIV-IN-EGFP virions were produced as previously
384 described (*34*) by performing polyethylenimine-mediated transfection of HEK293T cells with
385 6 µg of pVpr-IN-EGFP, 6 µg of HIV-1 NL4-3 non-infectious molecular clone (pD64E; NIH
386 AIDS Reagent Program 10180), and 1 µg of pVSV-G. The cells were incubated for 4 h before
387 the medium was replaced with fresh complete medium. Virion-containing supernatants were
388 collected after 48 h, filtered through a 0.45-µm syringe filter, and pelleted using the Lenti-X
389 Concentrator (631232; Clontech) according to the manufacturer's instructions. The multiplicity
390 of infection (MOI) of virus stocks was determined by transducing a known number of HeLa
391 cells with a known amount of virus particles and then counting GFP-positive cells using flow
392 cytometry. For luciferase reporter HIV-1 virus, the HIV-1 p24 antigen content in viral stock
393 were quantified using the HIV1 p24 ELISA kit (Abcam, ab218268), according to the
394 manufacturer's instruction. For virus infection, HeLa cells were seeded at a density of 0.5–4 ×

395 10^5 cells/mL on the day before infection. The culture medium was replaced with fresh complete
396 culture medium 2 hpi. The infected cells were washed twice with PBS and harvested at the
397 indicated time points. Jurkat cells were seeded at a density of 1×10^6 cells/mL and inoculated
398 with 300ng/p24 capsid antigen. The plates were centrifuged at 1000 *g* at 30°C for 1 h. The
399 medium was replaced with fresh RPMI 2 h after infection.

400 **Primary cell isolation, culture, T cell activation, and infection**

401 For $CD4^+$ T cells isolation, human PBMC (ST70025, STEMCELL Technologies) was mixed
402 and incubated with MACS CD4 MicroBeads (130-045-101, Miltenyi Biotec) and FITC-
403 conjugated mouse anti-CD4 (561005, BD Bioscience) according to the manufacturer's
404 instructions. Then the $CD4^+$ T cells were enriched by using LS Columns (130-042-401,
405 Miltenyi Biotec) and MidiMACS Separator (130-042-302, Miltenyi Biotec). The efficiency of
406 magnetic separation was analyzed by using Flow-Activated Cell Sorter Canto II (BD
407 Bioscience) and Flowjo software (Flowjo).

408 $CD4^+$ T cells were cultured in Roswell Park Memorial Institute (RPMI) 1640 medium (Gibco),
409 supplemented with 10% (v/v) fetal bovine serum (FBS, Cytiva), antibiotic mixture (100
410 units/ml penicillin–streptomycin, Gibco), 1% (v/v) GlutaMAX-I (Gibco), and 20 ng/ml of IL-
411 2 (PHC0026, Gibco), left in resting state or activated with Dynabeads Human T-Activator
412 CD3/CD28 (1161D, Thermo Fisher Scientific) for 72 h. $CD4^+$ T cells activation efficiency was
413 assessed by staining cells with FITC-conjugated mouse anti-CD25 (340694, BD Bioscience)
414 and APC-conjugated mouse anti-CD69 (130-114-046, Miltenyi Biotec) and using Flow-
415 Activated Cell Sorter Canto II (BD Bioscience) and Flowjo software (Flowjo).

416 Purified and activated $CD4^+$ T cells were seeded at a density of 1×10^6 cells/mL and inoculated
417 with 600ng/p24 capsid antigen in presence of polybrene. The plates were centrifuged at 1000

418 *g* at 30°C for 1 h. The medium was replaced with fresh RPMI 2 h after infection.

419 **DRIP-qPCR**

420 DRIP was performed as described for the construction of the DRIPc-seq library. After the
421 elution of isolated complexes, nucleic acids were purified using the standard phenol-
422 chloroform extract method and used for qPCR. S6 Table presents details of the primer
423 sequences used for DRIP-qPCR analysis.

424 **RNA-seq library construction**

425 For RNA-seq, HeLa cells were infected with VSV-G-pseudotyped HIV-1 NL4-3 ΔEnv EGFP
426 virus at a MOI of 0.6 and harvested at 0, 3, 6, and 12 hpi. Sequencing was performed with
427 biological replicates. Total RNA was extracted using TRIzol reagent (Invitrogen), according to
428 the manufacturer's instructions. An mRNA sequencing library was constructed using Illumina
429 adaptors harboring p5 and p7 sequences and Rd1 SP and Rd2 SP sequences. Sequencing was
430 performed using the HiSeq2500 system (Illumina).

431 **Luciferase assay**

432 HeLa cells infected with VSV-G-pseudotyped pNL4-3.Luc.R-E HIV-1 viruses were harvested
433 at 48 hpi, and luminescence was measured using the Dual-Luciferase Reporter Assay System
434 (Promega) according to the manufacturer's instructions. Briefly, 250 μl of passive lysis buffer
435 was used to lyse cells for each sample, 20 μl of the lysate was mixed with 100 μl of the
436 Luciferase Assay Reagent II, and the luminescence of firefly luciferase was measured using a
437 microplate luminometer (Berthold). The luminescence signal were normalized with total
438 protein content, measured by BCA assay.

439

440 **Quantitative real-time PCR (qPCR)**

441 For RT (reverse transcription)-qPCR, 1 μg of RNA was reverse-transcribed using the ReverTra
442 Ace qPCR RT Kit (TOYOBO) following the manufacturer's instructions. For qPCR, DNA
443 extracts were prepared using a DNA purification kit (Qiagen, 51106) according to the
444 manufacturer's instructions. Equivalent amounts of purified gDNA from each sample were
445 analyzed using qPCR. qPCR was performed using TOPreal qPCR PreMIX (Enzynomics,
446 RT500M). The reactions were performed in duplicate or triplicate for technical replicates. PCR
447 was performed using the iCycler iQ real-time PCR detection system (Bio-Rad). All the primers
448 used for qPCR are listed in S6 Table.

449 **DRIPc-seq library construction**

450 DRIP followed by library preparation, next-generation sequencing, and peak calling were
451 performed as described earlier (*29*). Briefly, the corresponding cells were harvested and their
452 gDNA was extracted. The extracted nucleic acids were fragmented using a restriction enzyme
453 cocktail with BsrB I (NEB, R0102S), HindIII (NEB, R0136L), Xba I (NEB, R0145L), and
454 EcoRI (NEB, R3101L) overnight at 37°C. Half of the fragmented nucleic acids were digested
455 with RNase H (New England Biolabs) overnight at 37°C to serve as a negative control. The
456 digested nucleic acids were cleaned using standard phenol-chloroform extraction and
457 resuspended in DNase/RNase-free water. DNA–RNA hybrids were immunoprecipitated from
458 total nucleic acids using mouse anti-DNA–RNA hybrid S9.6 (Kerafast, ENH001) DRIP
459 binding buffer and incubated overnight at 4°C. Dynabeads Protein A (Invitrogen, 10001D) was
460 used to pull down the DNA-antibody complexes by incubation for 4 h at 4°C. The isolated
461 complexes were washed twice with DRIP binding buffer before elution. For elution, the
462 isolated complexes were incubated in an elution buffer containing proteinase K for 45 min at

463 55 °C. Subsequently, DNA was purified using the standard phenol-chloroform extract method
464 and subjected to DNase I (Takara, 2270 B) treatment and reverse transcription for DRIPc-seq
465 library construction. DRIPc-seq was performed in biological replicates. S5 Table shows details
466 of the oligonucleotides used for DRIPc-seq library construction. DRIPc-seq libraries were
467 analyzed using 150 bp paired-end sequencing on a HiSeqX Illumina instrument.

468 **Immunofluorescence microscopy**

469 For immunofluorescence assays of S9.6 nuclear signals, when indicated, the cells were pre-
470 extracted with cold 0.5% NP-40 for 3 min on ice. Cells were fixed with 100% ice-cold methanol
471 for 10 min on ice and then incubated with 100% ice-cold acetone for 1 min. The slides were
472 washed three times with 1× PBS and incubated with or without 60 U/mL RNase H (M0297S,
473 NEB) at 37°C for 36 h or left untreated. The slides were subsequently briefly rinsed thrice with
474 2% BSA/0.05% Tween (in PBS) and incubated with mouse anti-DNA–RNA hybrid S9.6
475 (Kerafast, ENH001; 1:100) and rabbit anti-nucleolin (Abcam, ab22758; 1:300) in 2%
476 BSA/0.05% Tween (in PBS) for 4 h at 4°C. The slides were then washed three times with 2%
477 BSA/0.05% Tween (in PBS) and incubated with goat anti-rabbit AlexaFluor-488-conjugated
478 (Invitrogen, A-11008) and goat anti-mouse AlexaFluor-568-conjugated (Molecular Probes,
479 A11004) secondary antibodies (1:200) for 2 h at room temperature. The slides were then
480 washed three times with 2% BSA/0.05% Tween (in PBS) and mounted using the ProLong Gold
481 AntiFade reagent (Invitrogen). Images were obtained using an inverted microscope Nikon
482 Eclipse Ti2, equipped with a 1.45 numerical aperture, plan apochromat lambda 100× oil
483 objective, and an scientific complementary metal–oxide–semiconductor camera (Photometrics
484 prime 95 B 25 mm). For each field of view, images were obtained with DAPI395, GFP488,
485 and Alexa594 channels using the NIS-Elements software. For quantification analysis, binary

486 masks of nuclei and nucleoli were generated using the ROI manager and auto local thresholding
487 using the ImageJ software. The intensity of nuclear signals for DNA–RNA hybrids and
488 nucleolin was then quantified. The final DNA–RNA hybrid signals in the nucleus were
489 calculated by subtracting the nucleolin signals from the DNA–RNA hybrid signals.

490 **pgR-rich and -poor cell line generation with piggyBac transposition**

491 We adapted and modified an elegantly designed episomal system that induces defined R-loops
492 with controlled transcription levels (*17*) for R-loop-forming or non-R-loop-forming sequence
493 subcloning into the piggyBac transposon vector. HeLa cells were seeded at a density of 5×10^4
494 cells/ml in a 6-well plate. The next day, cells were transfected with 0.2 μg of Super PiggyBac
495 Transposase Expression Vector (System Biosciences, PB210PA-1) and 0.2, 1, or 2 μg of
496 transposon vectors with appropriate "cargo" sub cloned using Lipofectamine 3000 (Invitrogen)
497 according to the manufacturer's instructions. After 3 days, the cells were treated with 10 μg/ml
498 blasticidin S (Gibco, A1113903) for selection. Cells with positive integrants for more than 7
499 days were validated using immunoblotting or RT-qPCR following treatment with DOX. Jurkat
500 cells were seeded at a density of 8×10^5 cells/ml in a 6-well plate and transfected with 0.2 μg
501 of transposase and 1 μg of corresponding transposon vectors with Lipofectamine 3000, like
502 HeLa cells. After 3 days, the cells were treated with 10 μg/ml blasticidin S (Gibco, A1113903)
503 for selection. For each passage, cells were cushioned onto Ficoll-Pacque (Cytiva, 17144002)
504 to separate live cells from dead cell debris. The cells over the cushion were washed with PBS
505 and incubated in cell culture medium with 10 μg/ml of blasticidin for further selection for at
506 least 14 days. Cells with positive integrants were validated by immunoblotting after treatment
507 with DOX. Quantification of successfully integrated piggyBac transposons was performed
508 using a piggyBac qPCR copy number kit (System Biosciences, PBC100A-1).

509 **HIV-1 integration site sequencing library construction**

510 HIV-1 integration site sequencing library construction was performed as described earlier (*7,*
511 *9*). Summarily, HeLa cells and primary $CD4^+$ T cells were infected with VSV-G-pseudotyped
512 HIV-1 NL4-3 ΔEnv EGFP virus at a MOI of 0.6 and harvested 5 days post infection. gDNA
513 was isolated using a DNA purification kit (Qiagen, 51106), according to the manufacturer's
514 instructions. gDNA (10 µg) was digested overnight at 37°C with 100 U each of the restriction
515 endonucleases MseI (NEB, R0525L) and BglII (NEB, R0144L). Linker oligonucleotides,
516 which were compatible for ligation with the MseI-generated DNA ends, were ligated with
517 gDNA overnight at 12°C in reactions containing 1.5 µM ligated linker, 1 µg fragmented DNA,
518 and 800 U T4 DNA ligase (NEB, M0202S). Viral LTR–host DNA junctions were amplified
519 using semi-nested PCR with a unique linker-specific primer and LTR primers. The second
520 round of PCR was carried out with primers binding to the LTR and the linkers for next-
521 generation sequencing. Two PCRs were performed in parallel for the first round of PCR and
522 five PCRs were performed in parallel for the second round of PCR to enhance library diversity.
523 S7 Table presents details of the oligonucleotides used for HIV-1 integration site sequencing
524 library construction. HIV-1 integration site sequencing was performed in biological replicates.
525 Integration site libraries were analyzed using 150 bp paired-end sequencing on a HiSeqX
526 Illumina instrument.

527 **Co-immunoprecipitation of DNA–RNA hybrid**

528 DNA–RNA hybrid immunoprecipitation was performed as described earlier (*39*). Summarily,
529 non-crosslinked HeLa cells transfected with the pFlag-IN codon-optimized plasmid were lysed
530 in 85 mM KCl, 5 mM PIPES (pH 8.0), and 0.5% NP-40 for 10 min on ice, and then, the lysates
531 were centrifuged at 750 *g* for 5 min to pellet the nuclei. The pelleted nuclei were resuspended

532 in sodium deoxycholate, SDS, and sodium lauroyl sarcosinate in RSB buffer and were
533 sonicated for 10 min (Diagenode Bioruptor). Extracts were then diluted (1:4 in RSB + T buffer)
534 and subjected to immunoprecipitation with the S9.6 antibody overnight at 4°C. Antibody-
535 bound complexes were incubated with Protein A Dynabeads (Invitrogen) for 4 h at 4°C for
536 immunoprecipitation. Normal mouse IgG antibodies (Santa Cruz, sc-2025) were used as
537 negative controls. RNase A (Thermo Scientific, EN0531) was added during
538 immunoprecipitation at 0.1 ng RNase A per µg gDNA. Beads were washed four times with
539 RSB + T; twice with RSB, and eluted either in 2× LDS (Novex, NP0007), 100 mM DTT for
540 10 min at 70°C (for western blot), or 1% SDS and 0.1 M $NaHCO_3$ for 30 min at room
541 temperature (for DNA–RNA hybrid dot blot).

542 For co-immunoprecipitation of DNA–RNA hybrids with RNase H treatment, gDNA containing
543 RNA–DNA hybrids was isolated from HeLa cells transfected with a pFlag-IN codon-optimized
544 plasmid using a QIAmp DNA Mini Kit (Qiagen, 51304). gDNA was sonicated for 10 min
545 (Diagenode Bioruptor) and then treated with 5.5 U RNase H (NEB, M0297) per µg of DNA
546 overnight at 37 °C. A fraction of gDNA was stored as "nucleic acid input" for dot blot analysis.
547 gDNA was cleaned using standard phenol-chloroform extraction, resuspended in
548 DNase/RNase-free water, enriched for DNA–RNA hybrids using immunoprecipitation with the
549 S9.6 antibody (overnight at 4°C), isolated with Protein A Dynabeads (Invitrogen; 4 h at 4°C),
550 washed thrice with RSB+T. The immunoprecipitated complexes were incubated with nuclear
551 extracts of HeLa cells transfected with the pFlag-IN codon-optimized plasmid for 2 h at 4°C
552 with diluted HeLa nuclear extracts. The cell lysate containing proteins were pre-treated with
553 0.1 mg/ml RNase A (Thermo Scientific, EN0531) for 1 h at 37°C to degrade all RNA–DNA
554 hybrids, and the excess of RNase A was blocked by adding 200 U of SUPERase in RNase
555 inhibitor (Invitrogen, AM2694) for immunoprecipitation. In addition, 100 µL fraction of

556 diluted and RNase A pre-treated extracts prior to immunoprecipitation was stored as "protein
557 input" for western blotting. Beads were washed four times with RSB + T; twice with RSB, and
558 eluted either in 2× LDS (Novex, NP0007), 100 mM DTT for 10 min at 70°C (for western blot),
559 or 1% SDS, and 0.1 M $NaHCO_3$ for 30 min at room temperature (for DNA–RNA hybrid dot
560 blot).

561 **Recombinant Sso7d-IN protein purification**

562 Sso7d-integrase active site mutant E152Q was expressed in Escherichia coli BL21-AI and
563 purified essentially as previously described (*52*). Briefly, Sso7d-IN (E152Q) expressed BL21-
564 AI cells were lysis in lysis buffer (20 mM HEPES pH 7.5, 2 mM 2-mercaptoethanol, 1 M NaCl,
565 10% (w/v) glycerol, 20 mM imidazole, 1 mg RNase A, and 1000 U DNase I) and purified by
566 nickel affinity chromatography (Qiagen, 30210). Protein were first loaded on HeparinHP
567 column (GE Healthcare) equilibrated with equilibrated with 20 mM Tris, pH 8.0, 0.5 mM TCEP,
568 200 mM NaCl, 10% glycerol for anion exchange chromatography prior to the size exclusion
569 chromatography. Proteins were eluted with a linear gradient of NaCl from 200 mM to 1 M.
570 Eluted fractions were pooled and then separated on a Superdex-200 PC 10/300 GL column
571 (GE Healthcare) equilibrated with 20 mM Tris pH 8.0, 0.5 mM TCEP, 500 mM NaCl and 6%
572 (w/v) glycerol. The purified protein was concentrated to 0.6 mg/ml using an Amicon centrifugal
573 contentrator (EMD Millipore), flash-frozen in liquid nitrogen and stored at -80°C.

574 **Electrophoretic mobility shift assay for R-loop binding of Sso7d-IN**

575 To test the binding affinity of Sso7d-tagged HIV-1 IN to different types of nucleic acid
576 substrates, we prepared R-loop, dsDNA, RNA-DNA hybrid with exposed ssDNA
577 (R:D+ssDNA), RNA-DNA hybrid (Hybrid), ssDNA, and ssRNA by annealing different
578 combinations of Cy3, Cy5 or non-labeled oligonucleotides following the previous protocol (*53*).

579 10 nM of DNA substrate was incubated with Sso7d-IN at different concentrations in assembly
580 buffer (20 mM HEPES pH 7.5, 5 mM $CaCl_2$, 8 mM 2-mercaptoethanol, 4 uM $ZnCl_2$, 100 mM
581 NaCl, 25% (w/v) glycerol and 50 mM 3-(Benzyldimethylammonio) propanesulfonate (NDSB-
582 256)), for 1 h at 30°C then incubated for 15 min on ice. All the reactants were run on 4.5% non-
583 denaturing PAGE in 1× TBE and then Cy3 or Cy5 fluorescence signal was imaged by
584 ChemiDoc MP imaging system (Bio-Rad). S8 Table presents details of the oligonucleotide
585 sequence used for EMSA.

586 **PLA**

587 For PLA, HeLa cells were grown on coverslips and infected with HIV-IN-EGFP virions. At 6
588 hpi, cells were pre-extracted with cold 0.5% NP-40 for 3 min on ice. The cells were fixed with
589 4% paraformaldehyde in PBS for 15 min at 4 °C. The cells were then blocked with 1× blocking
590 solution (Merck, DUO92102) for 1 h at 37°C in a humidity chamber. After blocking, cells were
591 incubated with the following primary antibodies overnight at 4°C for S9.6-HIV-1-IN_PLA:
592 mouse anti-DNA–RNA hybrid S9.6 (1:250; Kerafast, ENH001) and rabbit anti-GFP (1:500;
593 Abcam, ab6556). The following day, after washing with once with buffer A twice (Merck,
594 DUO92102), cells were incubated with pre-mixed Duolink PLA plus (anti-mouse) and PLA
595 minus probes (anti-rabbit) antibodies for 1 h at 37°C. The subsequent steps in the proximal
596 ligation assay were performed using the Duolink PLA Fluorescence kit (Sigma) according to
597 the manufacturer's instructions. To obtain images, the mounted specimens were visually
598 scanned and representative images were acquired using a Zeiss LSM 710 laser scanning
599 confocal microscope (Carl Zeiss). The number of intranuclear PLA puncta was quantified using
600 the ImageJ software. For each biological replicate and experiment, a PLA with a single
601 antibody was performed as a negative control under the same conditions.

602 **DRIPc-Seq data processing and peak calling**

603 DRIPc-seq reads were quality-controlled using FastQC v0.11.9 (*54*), and sequencing adapters
604 were trimmed using Trim Galore! v0.6.6 (*55*) based on Cutadapt v2.8 (*56*). Trimmed reads
605 were aligned to the hg38 reference genome using bwa v0.7.17-r1188 (*57*). Read deduplication
606 and peak calling were performed using MACS v2.2.7.1 (*58*). Because R-loops appear as both
607 narrow and broad peaks in DRIPc-seq read alignment owing to its variable length, two
608 independent "MACS2 callpeak" runs were performed for narrow and broad peak calling. The
609 narrow and broad peaks were merged using Bedtools v2.26.0 (*59*). To increase the sensitivity
610 of DRIPc-seq peak identification, peaks were called after pooling the two biological replicates
611 of the DRIPc-seq sequencing data for each condition.

612 **Consensus R-loop peak calling**

613 The R-loop peaks at 0, 3, 6 and 12 hpi were first merged using "bedtools merge" to create a
614 universal set of R-loop peaks across time points (n = 46542). Then, each of the universal R-
615 loop peaks was tested for overlap with the R-loop peaks for 0, 3, 6 and 12 hpi using "bedtools
616 intersect". In all, 9,190, 21,403, 33,544, and 9,941 peaks overlapped with 0, 3, 6, and 12 hpi
617 R-loop peaks, respectively. For CD4 cells, we identified a universal R-loop set consisting of
618 3,928 R-loops, and among them, 737, 722, 1,796 and 2,766 peaks overlapped with 0, 3, 6 and
619 12hpi R-loop peaks.

620 **HIV-1 integration site sequencing data processing**

621 Quality control of HIV-1 integration site-sequencing reads was performed using FastQC
622 v0.11.9. To discard primers and linkers specific for integration site-sequencing from reads, we
623 used Cutadapt v2.8 with the following option: "-u 49 -U 38 --minimum-length 36 --pair-filter

624 any --action trim -q0,0 –a linker -A TGCTAGAGATTTTCCACACTGACTGGGTCTGAGGG
625 -A GGGTCTGAGGG --no-indels --overlap 12". This allowed the first position of the read
626 alignment to directly represent the genomic position of HIV-1 integration. Processed reads
627 were aligned to the hg38 reference genome using bwa v0.7.17-r1188, and integration sites were
628 identified using an in-house Python script. Genomic positions supported by more than five read
629 alignments were regarded as HIV-1 integration sites. For Jurkat cells, we adopted integration
630 site sequencing data of HIV-1 infected wild type Jurkat cells from SRR12322252 (*60*).

631 **Co-localization analysis of R-loops and integration sites**

632 Enrichment of integration sites near the R-loop peaks was tested using a randomized
633 permutation test. Randomized R-loop peaks were generated using "bedtools shuffle" command,
634 thus preserving the number and the length distribution of the R-loop peaks during the
635 randomization process. Similarly, integration sites were randomized using the "bedtools shuffle"
636 command. Randomization was performed 100 times. ENCODE blacklist regions (*61*) were
637 excluded while shuffling the R-loops and integration sites to exclude inaccessible genomic
638 regions from the analysis. For each of the observed (or randomized) integration sites, the
639 closest observed (or randomized) R-loop peak and the corresponding genomic distance were
640 identified using the "bedtools closest" command. The distribution of the genomic distances
641 was displayed to show the local enrichment of integration sites in terms of the increased
642 proportion of integration sites within the 30-kb window centered on R-loops compared to their
643 randomized counterparts.

644 **DNA plasmid construction and transfection**

645 R-loop-forming mAIRN and non-R-loop forming ECPF sequences were subcloned from
646 pSH26 and pSH36 plasmids, which were generously provided by Prof. Karlene A. Cimprich,

647 into the piggyBac transposon vector, where the tet operator sequences were located upstream
648 of the minimal CMV promoter. The pFlag-IN codon-optimized plasmid and pVpr-IN-EGFP
649 were kindly provided by Prof. A. Engelman and Prof. Anna Cereseto, respectively.
650 Lipofectamine 3000 (Invitrogen) transfection reagent was used for the transfection of all
651 plasmids into cells, according to the manufacturer's protocol.

652 **DNA–RNA hybrid dot blotting**

653 Total gDNA was extracted using the QIAmp DNA Mini Kit (Qiagen, 51304) according to the
654 manufacturer's instructions. gDNA (1.2 μg) was treated with 2 U RNase H (NEB, M2097) per
655 μg of gDNA for 4 h at 37°C, with half of the sample left untreated but denatured. Half of the
656 DNA sample was probed with S9.6 antibody (1:1000), and the other half was probed with an
657 anti-ssDNA antibody (MAB3034, Millipore, 1:10000).

658 **Immunoblotting**

659 Cells were lysed using RIPA buffer (50 mM Tris, 150 mM sodium chloride, 0.5% sodium
660 deoxycholate, 0.1% SDS, and 1.0% NP-40) supplemented with 10 μM leupeptin (Sigma-
661 Aldrich) and 1 mM phenylmethanesulfonyl fluoride (Sigma-Aldrich) and boiled at 98°C for
662 10 min with SDS sample buffer prior to SDS-PAGE. The primary antibodies used were mouse
663 monoclonal anti-FLAG M2 (Sigma, F3165), monoclonal mouse anti-HSC70 (Abcam, ab2788),
664 polyclonal rabbit anti-histone H3 (tri methyl K4) antibody (Abcam, ab8580), monoclonal
665 mouse anti- HIV-1 Integrase (Santa Cruz, sc-69721), rabbit anti-LaminA/C antibody (Cell
666 Signaling, 2032), and monoclonal mouse anti-Actin (Invitrogen, MA1-744). All primary
667 antibodies were used at a dilution of 1:1000 for western blotting. Peroxidase-conjugated anti-
668 mouse IgG (115-035-062) and anti-rabbit IgG (111-035-003; both Jackson Laboratories) were
669 used as secondary antibodies at 1:5000 dilution. Signals were detected using the SuperSignal

West Pico chemiluminescence kit (Thermo Fisher Scientific).

RNA-seq data processing

RNA-seq reads were quality-controlled and adapter-trimmed as in DRIPc-seq processing. To quantify the expression levels of protein-coding genes, processed reads were aligned to the hg38 reference genome with GENCODE v37 gene annotation (*62*) using STAR v2.7.3a (*63*). Gene expression quantification was performed using RSEM v1.3.1. To quantify the expression levels of transposable elements (TEs), we used TEtranscripts v2.2.1 (*64*). Processed reads were first aligned to the hg38 reference genome using GENCODE v37 and RepeatMasker TE annotation using STAR v2.7.3a. In this case, STAR options were modified as follows to utilize multimapping reads in downstream analyses: "--outFilterMultimapNmax 100 --winAnchorMultimapNmax 100 --outMultimapperOrder random --runRNGseed 77 --outSAMmultNmax 1 --outFilterType BySJout --alignSJoverhangMin 8 --alignSJDBoverhangMin 1 --alignIntronMin 20 --alignIntronMax 1000000 --alignMatesGapMax 1000000". Expression levels of TEs were quantified as read counts with the "TEcount" command.

Genome annotations

All bioinformatic analyses were performed using the hg38 reference genome and GENCODE v37 gene annotation. Promoters were defined as a 2-kb region centered at the transcription start sites of the APPRIS principal isoform of protein-coding genes. TTS regions were defined as the 2-kb region centered at the 3′ terminals of protein-coding transcripts. CpG island annotations were downloaded from the UCSC table browser. CpG shores were defined as 2-kb regions flanking CpG islands, excluding the regions overlapping with CpG islands. Similarly, CpG shelves were defined as 2-kb regions flanking the stretch of CpG islands and shores while

693 excluding the regions overlapping with CpG islands and shores. Annotations for LINE, SINE,
694 and LTR were extracted from the RepeatMasker track in the UCSC table browser.

695 **Identification of viral sequencing reads in DRIPc-seq**

696 To identify sequencing reads originating from the viral genome, we aligned DRIPc-seq reads
697 to a composite reference genome consisting of the human and HIV1 genome (Genbank
698 accession number: AF324493.2) and computed the proportion of the reads mapped to HIV1
699 genome.

700 **Code availability**

701 Bioinformatics pipelines and scripts used in this study are accessible from
702 https://github.com/dohlee/hiv1-rloop.

703

Acknowledgements

We are grateful to Prof. Karlene A. Cimprich (Standford University) for providing the pSH26 and pSH36 plasmids, Prof. A. Engelman (Harvard Medical School) for providing pFlag-IN codon optimized plasmid and Prof. Anna Cereseto (University of Trento) for providing pVpr-IN-EGFP. The NL4-3 ΔEnv EGFP and pNL4-3.Luc.R-E- viral plasmids were obtained through the NIH HIV Reagent Program, Division of AIDS, NIAID, NIH. We thank Dr. Sungchul Kim (IBS center for RNA Research) and Seongjin An (Korea University) for their technical support in recombinant protein purification.

Author contributions

K.P. and K.A. designed experiments. K.P., J.J and S.L. performed experiments. D.L. performed the bioinformatical and statistical analyses. K.P., D.L., K.A. and S.K. analyzed the data. K.P., D.L., and K.A. wrote the manuscript.

Funding

This work was supported by the Institute for Basic Science of the Ministry of Science Grant (IBS-R008-D1) and the National Research Foundation of Korea (NRF) grant funded by the Korea government (NRF-2020R1A2C3011298) (to K. A.) and (NRF-2020R1A5A1018081) (to K.A.). The funders had no role in the study design, data collection, analysis, decision to publish, or preparation of the manuscript.

Competing interests

The authors have declared that no competing interests exist.

725 **Figures**

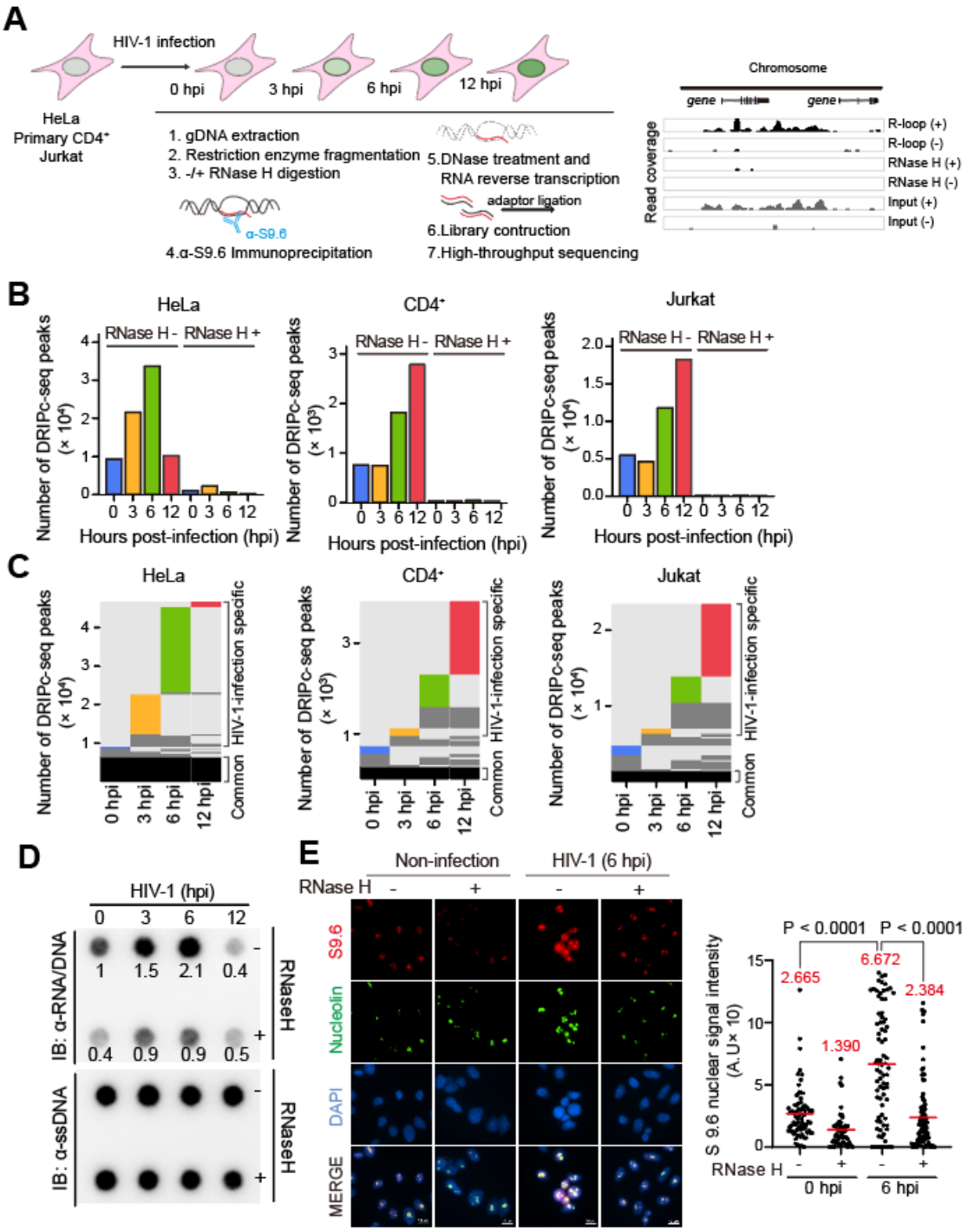

726

727

728 **Fig 1. HIV-1 infection induces genomic R-loop accumulation in cells at early post-infection.** (**A**) Summary
729 of experimental design for DRIPc-seq in HeLa cells, primary $CD4^+$ T cells and Jurkat cells infected with HIV-1.
730 (**B**) Bar graphs indicating DRIPc-seq peak counts for HIV-1-infected HeLa cells, primary $CD4^+$ T cells and Jurkat
731 cells harvested at the indicated hours post infection (hpi). Pre-immunoprecipitated samples were untreated (−) or
732 treated (+) with RNase H, as indicated. Each bar corresponds to pooled datasets from two biologically independent
733 experiments. (**C**) All genomic loci overlapping a DRIPc-seq peak from HIV-1 infected HeLa cells, primary $CD4^+$
734 T cells and Jurkat cells in at least one sample are stacked vertically; the position of each peak in a stack is constant
735 horizontally across samples. Each hpi occupies a vertical bar, as indicated. Each bar corresponds to pooled datasets
736 from two biologically independent experiments. Common peaks for all samples are represented in black, and in
737 dark gray for those common for at least two samples. The lack of a DRIP signal over a given peak in any sample
738 is shown in light gray. The sample-unique peaks are colored blue, yellow, green, and red at 0, 3, 6, and 12 hpi,
739 respectively. (**D**) Dot blot analysis of the R-loop in gDNA extracts from HIV-1 infected HeLa cells with MOI of
740 0.6 harvested at the indicated hpi. gDNAs were probed with anti-S9.6. gDNA extracts were incubated with or
741 without RNase H in vitro before membrane loading (anti-RNA/DNA signal). Fold-induction was normalized to
742 the value of harvested cells at 0 hpi by quantifying the dot intensity of the blots and calculating the ratios of the
743 S9.6 signal to the total amount of gDNA (anti-ssDNA signal). (**E**) Representative images of the
744 immunofluorescence assay of S9.6 nuclear signals in HIV-1 infected HeLa cells with MOI of 0.6 harvested at 6
745 hpi. The cells were pre-extracted of cytoplasm and co-stained with anti-S9.6 (red), anti-nucleolin antibodies
746 (green), and DAPI (blue). The cells were incubated with or without RNase H in vitro before staining with anti-
747 S9.6 antibodies, as indicated. Quantification of S9.6 signal intensity per nucleus after nucleolar signal subtraction
748 for the immunofluorescence assay. The mean value for each data point is indicated by the red line. Statistical
749 significance was assessed using one-way ANOVA ($n > 53$).

750

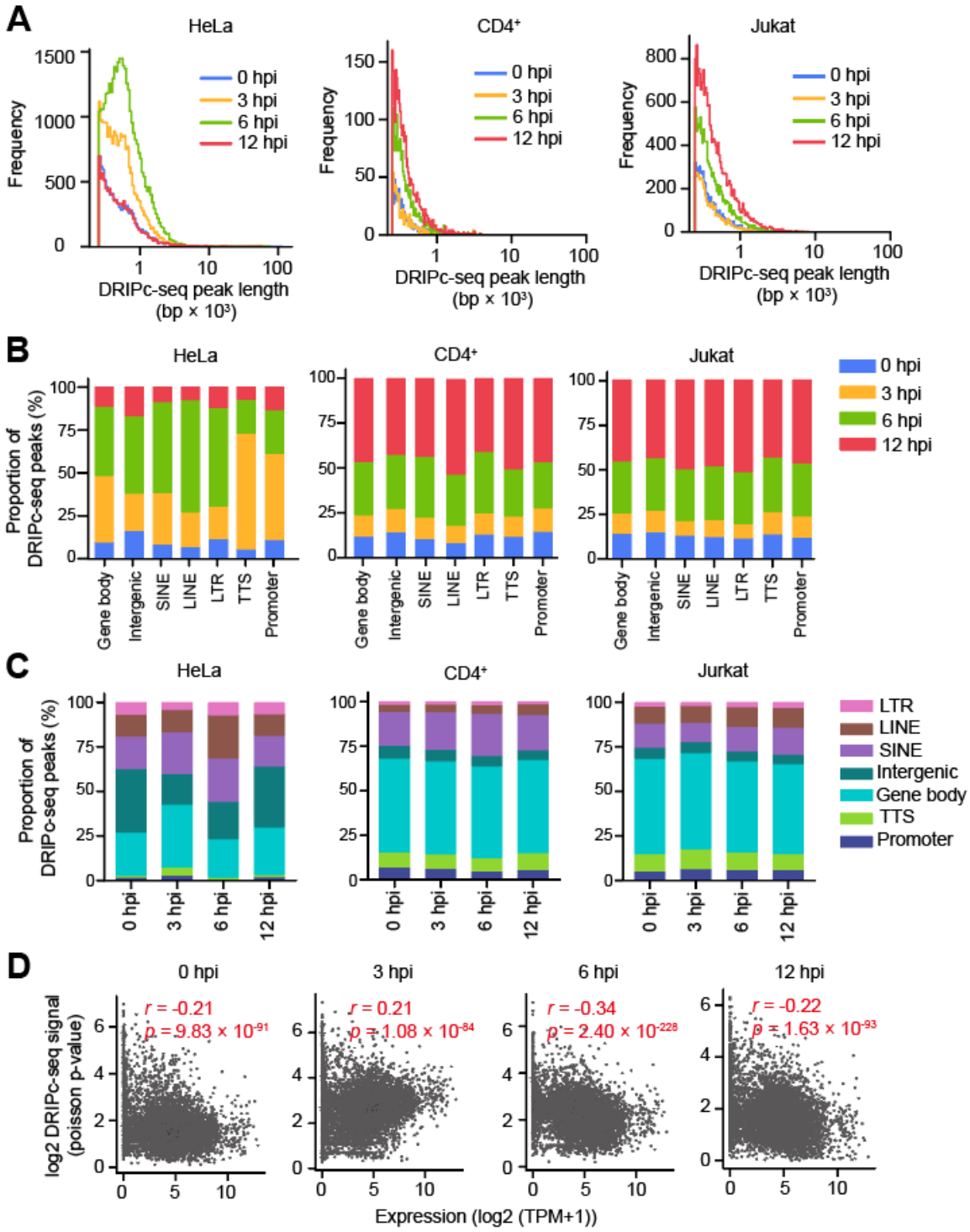
A
HeLa
CD4+
Jukat
Frequency
0 hpi
3 hpi
6 hpi
12 hpi
DRIPc-seq peak length
(bp × 10³)
B
Proportion of
DRIPc-seq peaks (%)
Gene body
Intergenic
SINE
LINE
LTR
TTS
Promoter
C
Jurkat
LTR
LINE
SINE
Intergenic
Gene body
TTS
Promoter
D
r = -0.21
p = 9.83 × 10-91
r = 0.21
p = 1.08 × 10-84
r = -0.34
p = 2.40 × 10-228
r = -0.22
p = 1.63 × 10-93
log2 DRIPc-seq signal
(poisson p-value)
Expression (log2 (TPM+1))

751

752

753 **Fig. 2. HIV-1-induced R-loops are enriched at both transcriptionally active and silent regions.** (**A**)
754 Distribution of DRIPc-seq peak lengths for HIV-1-infected HeLa cells, primary $CD4^+$ T cells and Jurkat cells
755 harvested at the indicated time points (blue, 0 hpi; yellow, 3 hpi; green, 6 hpi; red, 12 hpi). (**B**) Stacked bar graphs
756 indicating the proportion of DRIPc-seq peaks mapped for HIV-1-infected HeLa cells, primary $CD4^+$ T cells and
757 Jurkat cells harvested at the indicated hpi over different genomic features. (**C**) Stacked bar graphs indicating the
758 proportion of DRIPc-seq peaks mapped to indicated genomic compartments for HIV-1-infected HeLa cells,
759 primary $CD4^+$ T cells and Jurkat cells harvested at the 0, 3, 6, and 12 hpi . (**D**) Correlation between gene expression
760 and DRIPc-seq signals of HIV-1-infected HeLa cells with MOI of 0.6 harvested at the indicated hpi. Statistical
761 significance was assessed using Pearson's r and p-values.

762

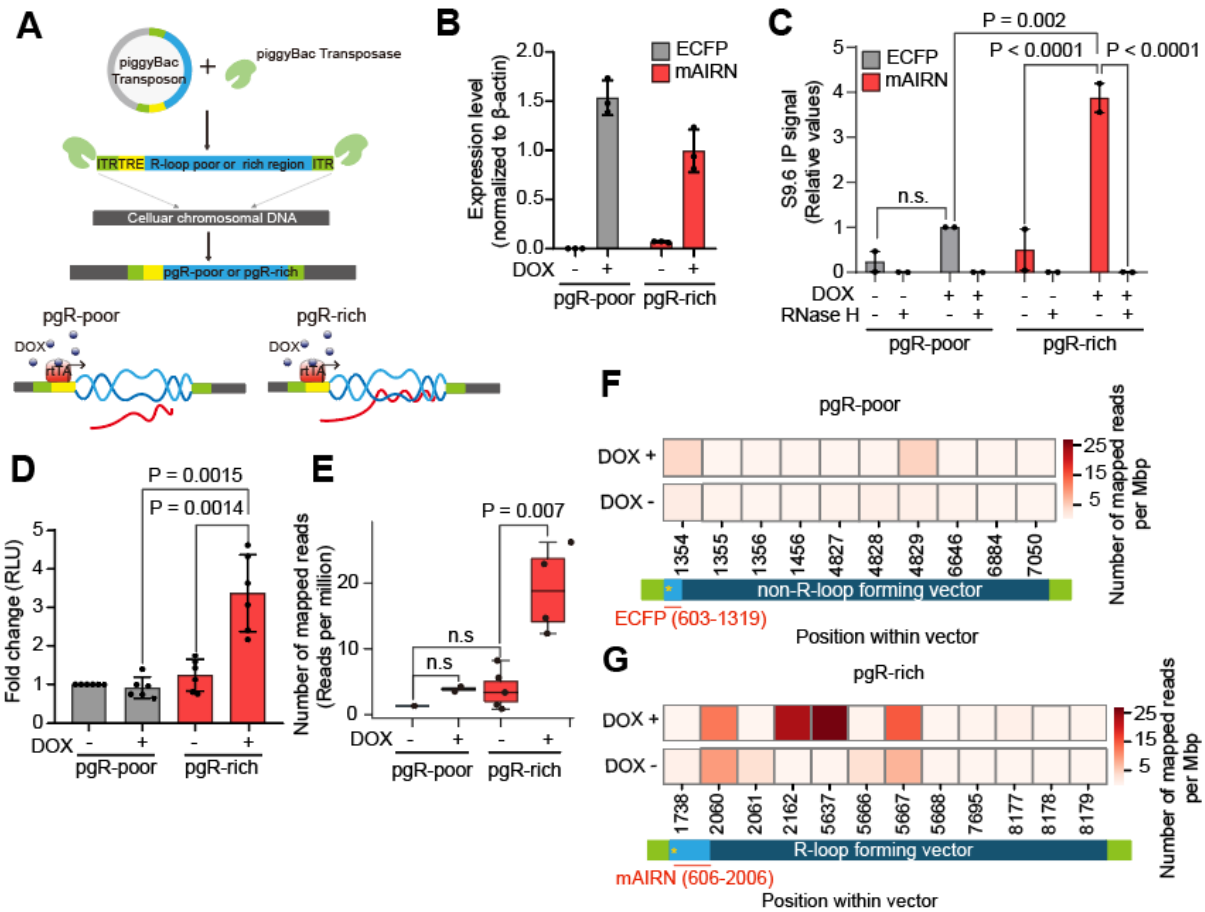

Fig. 3. R-loop inducible cell line model directly addresses R-loop-mediated HIV-1 integration site selection. (**A**) Summary of the experimental design for R-loop inducible cell lines, pgR-poor and pgR-rich. (**B**) Gene expression of ECFP (gray) and mAIRN (red), as measured using RT-qPCR in pgR-poor or pgR-rich cells. Where indicated, the cells were incubated with 1 μg/ml DOX for 24 h. Gene expression was normalized relative to *β-actin*. Data are presented as the mean ± SEM, n = 3. (**C**) DRIP-qPCR using the anti-S9.6 antibody against ECFP and mAIRN in pgR-poor or pgR-rich cells. Where indicated, the cells were incubated with 1 μg/ml DOX for 24 h. Pre-immunoprecipitated samples were untreated or treated with RNase H as indicated. Values are relative to those of DOX-treated (+) RNase H-untreated (−) pgR-poor cells. Data are presented as the mean ± SEM; statistical significance was assessed using two-way ANOVA (n = 2). (**D**) Bar graphs indicate luciferase activity at 48 hpi in pgR-poor or prR-rich cells infected with 100ng/p24 capsid antigen of luciferase reporter HIV-1 virus per 1× 10^5 cells/mL. Data are presented as the mean ± SEM; P values were calculated using one-way ANOVA (n = 6). (**E**) Box graph indicating the quantified HIV-1 integration site sequencing read count across pgR-poor and pgR-rich transposon sequences in untreated (–) or DOX-treated (+) pgR-poor or pgR-rich cell line infected with 100ng/p24

capsid antigen of luciferase reporter HIV-1 virus per 1×10^5 cells/mL. Each bar corresponds to pooled datasets from three biologically independent experiments (n =3). In each boxplot, the centerline denotes the median, the upper and lower box limits denote the upper and lower quartiles, and the whiskers denote the 1.5 × interquartile range. Statistical significance was assessed using a two-sided Mann–Whitney U test. (**F** and **G**) Heat maps representing the number of HIV-1 integration-seq mapped read across pgR-poor (**F**) or pgR-rich (**G**) transposon sequence in untreated (-) or DOX-treated (+) pgR-poor (**F**) or pgR-rich (**G**) cell line. Each rectangular box corresponds to the pooled the number of HIV-1 integration-seq mapped read from three biologically independent experiments (n =3) at the indicated position within pgR-poor (**F**) or pgR-rich (**G**) transposon vector. Each light blue box represents actual position of R-loop forming or non-R-loop forming sequence (ECFP or mAIRN) and the yellows stars indicate TRE promoter position within vector.

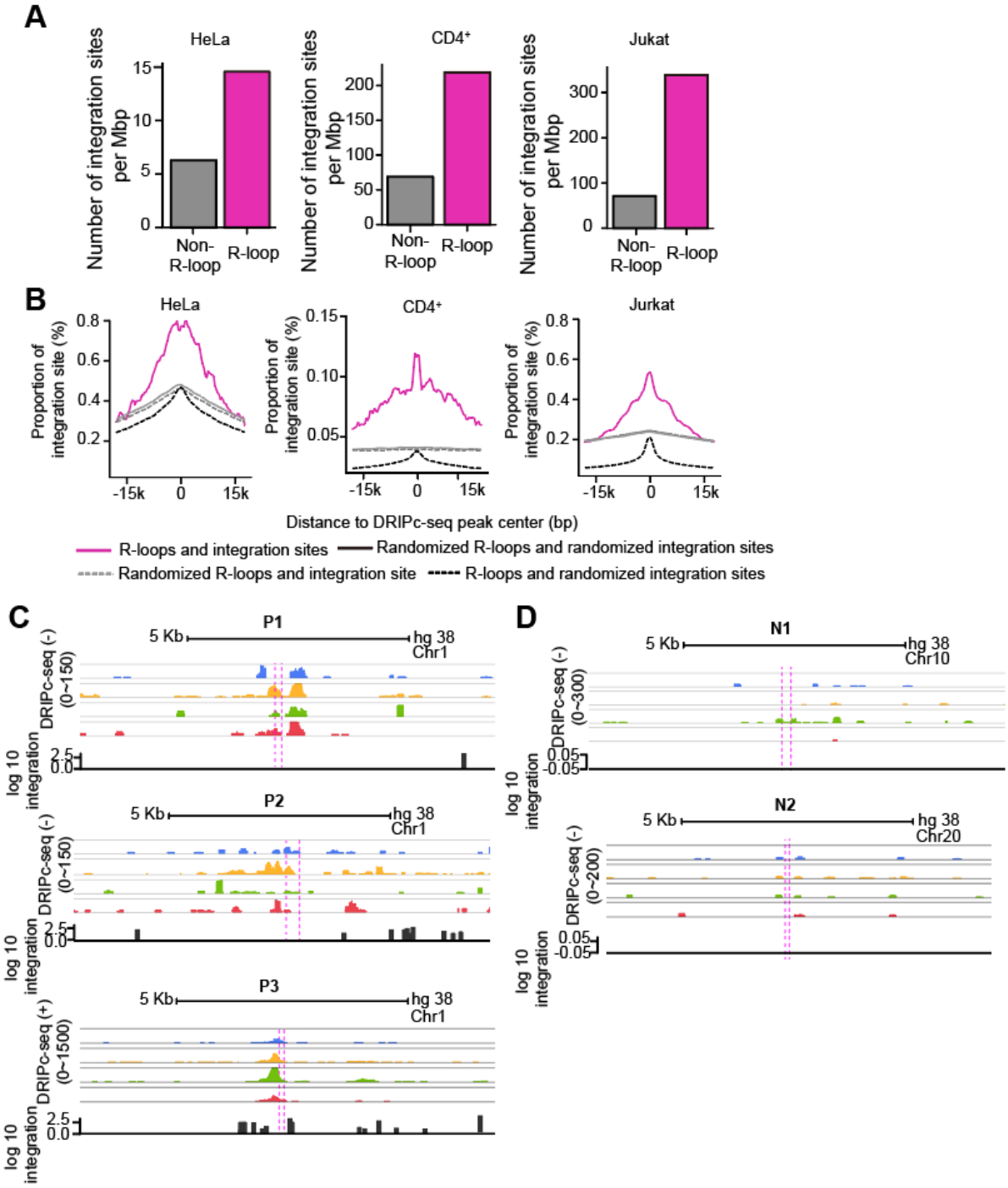

Fig. 4. HIV-1 prefers host genomic R-loop regions for its viral cDNA integration. (**A**) Bar graphs showing quantified number of HIV-1 integration sites per Mb pairs in total regions of 30-kb windows centered on DRIPc-seq peaks from HIV-1 infected HeLa cells, primary CD4$^+$ T cells and Jurkat cells (magenta) or non-R-loop region in the cellular genome (gray). (**B**) Proportion of integration sites within the 30-kb windows centered on DRIPc-

seq peaks (magenta solid lines) or randomized DRIPc-seq peaks (gray dotted lines). Control comparisons between randomized integration sites with DRIPc-seq peaks and randomized DRIPc-seq peaks are indicated by black dotted lines and gray solid lines, respectively. (**C** and **D**) Superimpositions of HIV-1-induced R-loop positive chromatin regions, P1-P3 (**C**), and HIV-1-induced R-loop negative chromatin regions, N1 and N2 (**D**), on DRIPc-seq (blue, 0 hpi; yellow, 3 hpi; green, 6 hpi; red, 12 hpi) and number of mapped read of HIV-1 integration-seq (integration, black). Magenta dotted lines represent primer binding sites in qPCR following DRIP.

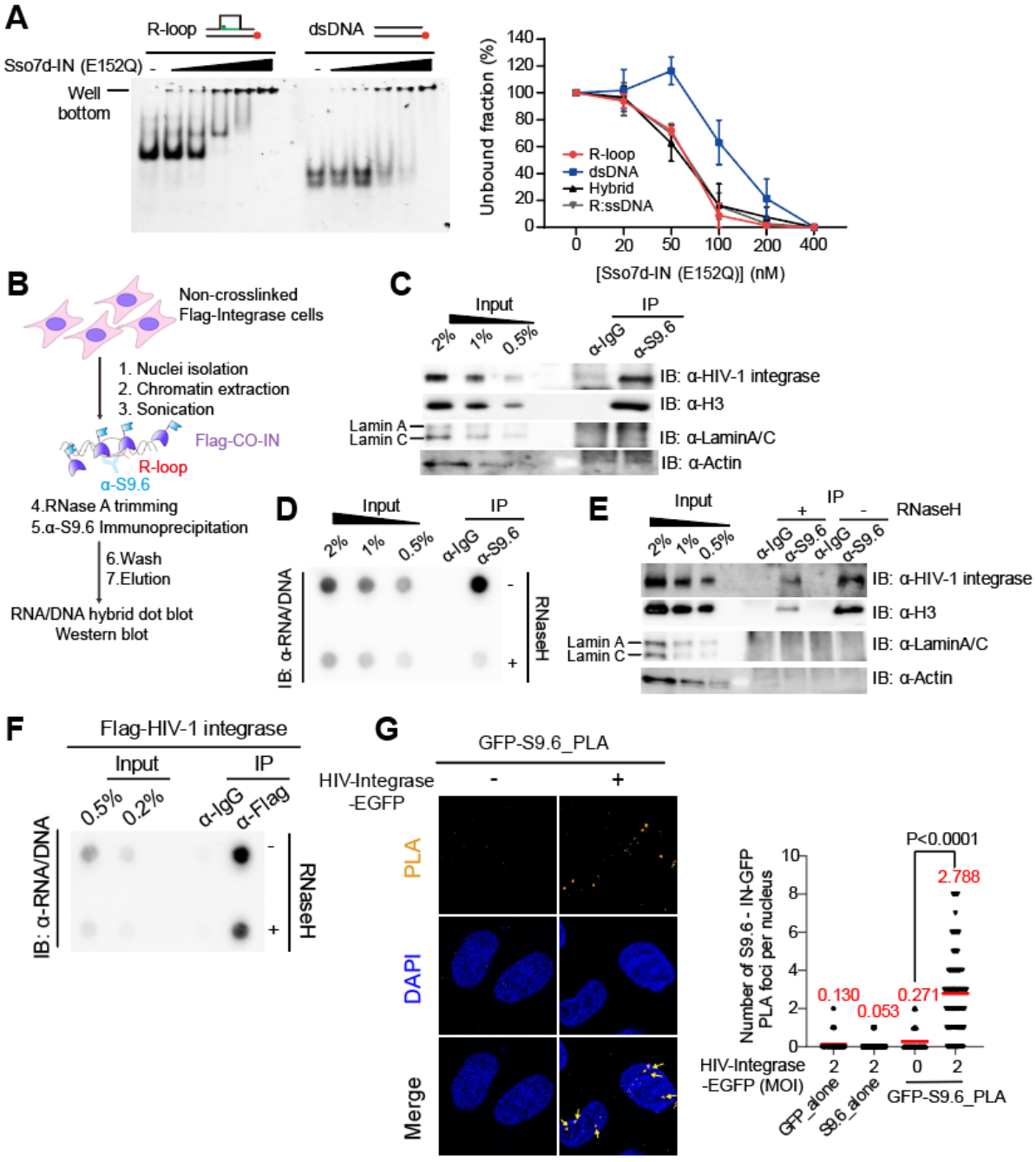

Fig. 5. HIV-1 integrase proteins directly bind to host genomic R-loops. (**A**) Representative gel images for EMSA of Sso7d-tagged HIV-1-integrase (E152Q) with R-loop and dsDNA, 10 nM nucleic acid substrate was incubated with Sso7d-tagged HIV-1-integrase (E152Q) at 0 nM, 20 nM, 50 nM, 100 nM, 200 nM, and 400 nM (left). Unbound fraction were quantified for EMSA of Sso7d-tagged HIV-1-integrase (E152Q) with different types substrates (R-loop, dsDNA, R-loop, R:D+ssDNA and Hybrid). Data are presented as the mean ± SEM, n = 3 (right). (**B**) Summary of the experimental design for R-loop immunoprecipitation using S9.6 antibody in FLAG-

807 tagged HIV-1 integrase protein-expressing HeLa cells. (**C**) Western blotting for HIV-1 integrase protein, H3, and
808 LaminA/C of DNA–RNA hybrid immunoprecipitation using the S9.6 antibody. (**D**) **and** (**E**) HeLa gDNA input
809 was either untreated (–) or treated (+) with RNase H before enrichment for DNA–RNA hybrids using the S9.6
810 antibody. gDNA–RNA hybrids were incubated with nuclear extracts depleted of DNA–RNA hybrids with RNase
811 A followed by S9.6 immunoprecipitation. DNA–RNA hybrid dot blot (**D**) and western blot of DNA–RNA hybrid
812 immunoprecipitation, probed with the indicated antibodies (**E**). (**F**) DNA–RNA hybrid dot blot of FLAG antibody-
813 immunoprecipitated nucleic acid extracts. Where indicated, nucleic acid extracts were untreated (–) or treated (+)
814 with RNase H before probing with the S9.6 antibodies. (**G**) Representative images of the proximity-ligation assay
815 (PLA) between GFP and S9.6 antibodies in HIV-IN-EGFP virion-infected HeLa cells at 6 hpi. Cells were
816 subjected to PLA (orange) and co-stained with DAPI (blue). PLA puncta in the nucleus are indicated by the yellow
817 arrows. Quantification analysis of number of PLA foci per nucleus (left). GFP_alone and S9.6_alone were used
818 as single-antibody controls from HIV-IN-EGFP virion-infected HeLa cells (right). The mean value for each data
819 point is indicated by the red line. P value was calculated using a two-tailed unpaired *t*-test ($n > 50$).

820

821 **Supplemental Information**

822 Materials and Methods

823 S1 Fig. Primary $CD4^+$ T cells sorting strategies and GFP-HIV-1 infection

824 S2 Fig. Genome browser screenshot over the HIV-1-induced R-loop forming positive or
825 negative genomic regions

826 S3 Fig. Host cellular R-loop induction by HIV-1 infection is host-genome specific.

827 S4 Fig. R-loop induction by HIV-1 infection does not follow transcriptome changes in HeLa
828 cells

829 S5 Fig. PiggyBac transposon-transposase insertion of R-loop forming and non-R-loop forming
830 sequences in HeLa cells

831 S6 Fig. HIV-1 integrase proteins directly binds to host genomic R-loops

832 S1 Table. Chromosomal position and DRIPc-seq signal for referenced R-loop-positive and –
833 negative regions in HIV-1 infected HeLa cells

834 S2 Table. Chromosomal position and DRIPc-seq signal for referenced R-loop-positive and –
835 negative regions in HIV-1 infected primary $CD4^+$ T cells

836 S3 Table. Chromosomal position and DRIPc-seq signal for referenced R-loop-positive and –
837 negative regions in HIV-1 infected Jurkat cells

838 S4 Table. RNA-seq analysis of relative gene expression levels of P1-3 and N1,2 R-loop regions

839 S5 Table. Oligonucleotides used for DRIPc-seq library construction

840 S6 Table. Primers used for qPCR

841 S7 Table. Oligonucleotides used for HIV-1 integration site sequencing library construct

842 S8 Table. Oligonucleotides used for electrophoretic mobility shift assay substrate preparation

843 S9 Table. Accession numbers and data sources.

844

845 # Supplementary figures

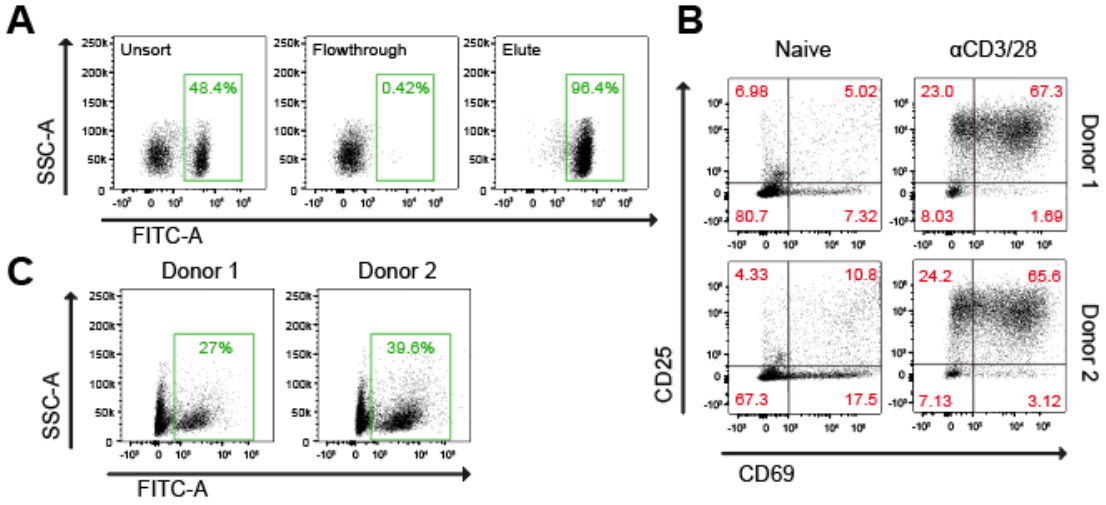

846

847 **S1 Fig. Primary CD4^{+} T cells sorting strategies and GFP-HIV-1 infection.** (**A**) Gating strategy used to
848 determine the efficiency of CD4^{+} T cells sorting from human PBMC. Pre-sorted PBMCs were staining with FITC-
849 conjugated anti-CD4 and subjected for positive CD4+ T cell sorting. The percentages of FITC stained cell
850 population at each step of cell sorting are as indicated. (**B**) Gating strategy used to determine non-activated (Naïve)
851 and activated cells (αCD3/28) with two markers, CD25 (FITC) and CD69 (APC), for each donor (upper panels,
852 Donor 1; lower panels, Donor 2). (**C**) Gating strategy used to determine HIV-1-infectivity of CD4+ T cells from
853 each donor infected with GFP reporter HIV-1 virus at 48 hpi. The percentages of GFP positive cell population at
854 are as indicated.

855

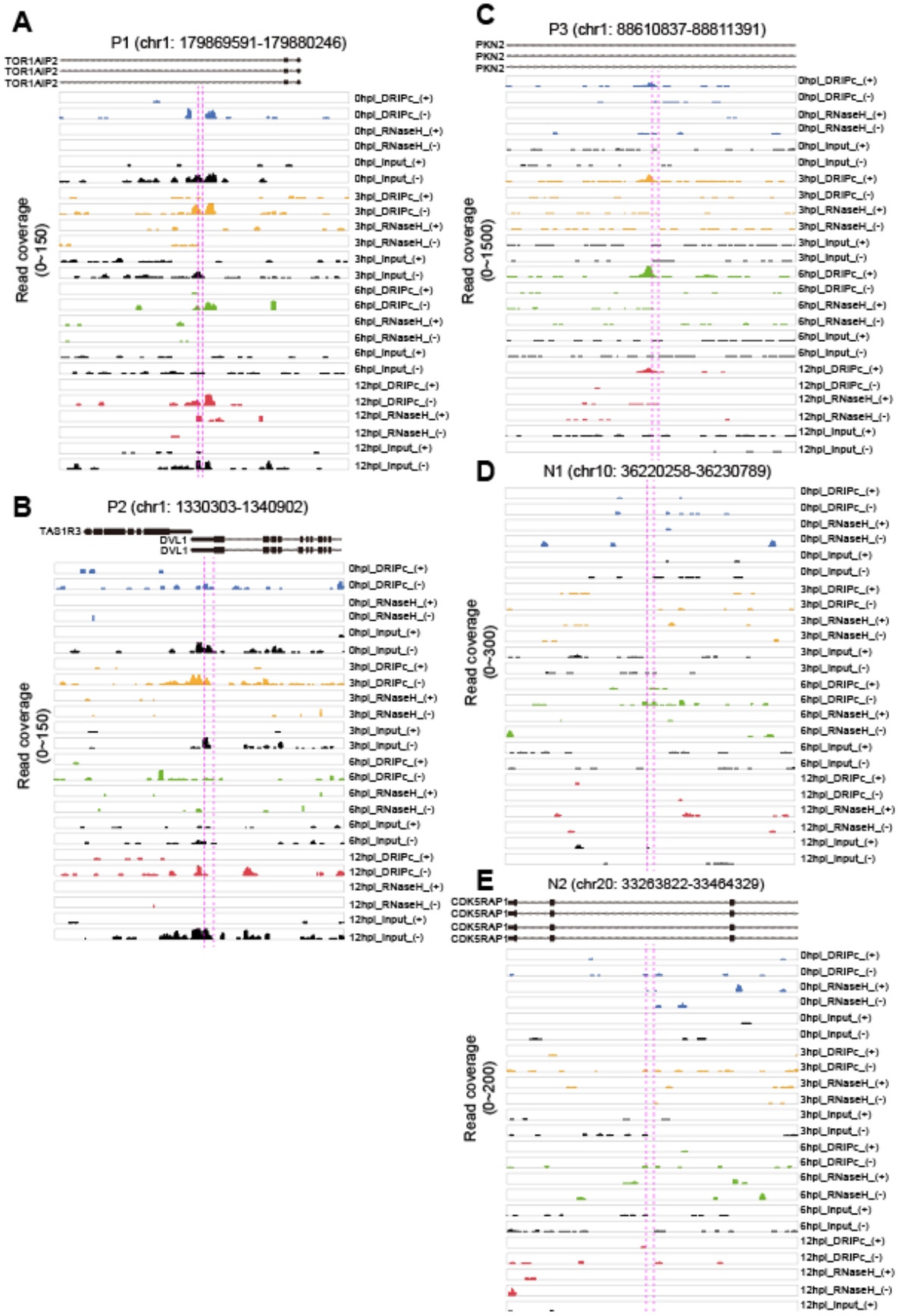
A
P1 (chr1: 179869591-179880246)
TOR1AIP2
TOR1AIP2
TOR1AIP2
Read coverage (0~150)
0hpI_DRIPc_(+)
0hpI_DRIPc_(-)
0hpI_RNaseH_(+)
0hpI_RNaseH_(-)
0hpI_Input_(+)
0hpI_Input_(-)
3hpI_DRIPc_(+)
3hpI_DRIPc_(-)
3hpI_RNaseH_(+)
3hpI_RNaseH_(-)
3hpI_Input_(+)
3hpI_Input_(-)
6hpI_DRIPc_(+)
6hpI_DRIPc_(-)
6hpI_RNaseH_(+)
6hpI_RNaseH_(-)
6hpI_Input_(+)
6hpI_Input_(-)
12hpI_DRIPc_(+)
12hpI_DRIPc_(-)
12hpI_RNaseH_(+)
12hpI_RNaseH_(-)
12hpI_Input_(+)
12hpI_Input_(-)
B
P2 (chr1: 1330303-1340902)
TAS1R3
DVL1
DVL1
Read coverage (0~150)
C
P3 (chr1: 88610837-88811391)
PKN2
PKN2
PKN2
Read coverage (0~1500)
D
N1 (chr10: 36220258-36230789)
Read coverage (0~300)
E
N2 (chr20: 33263822-33464329)
CDK5RAP1
CDK5RAP1
CDK5RAP1
CDK5RAP1
Read coverage (0~200)

856

857 **S2 Fig. Genome browser screenshot over the HIV-1-induced R-loop forming positive or negative genomic**
858 **regions. (A-C),** Genome browser screenshot over the P1 (**A**), P2 (**B**), and P3 (**C**) HIV-1 induced R-loop-positive
859 chromosomal regions showing result from DRIPc-seq in HIV-1-infected HeLa cells (blue, 0 hpi; yellow, 3 hpi;
860 green, 6 hpi; red, 12 hpi; black, input signals for each indicated sample) on plus (+) or minus (-) DNA strand.
861 Magenta dotted lines represent primer binding sites in qPCR following DRIP. **(D** and **E),** Genome browser
862 screenshot over the N1 (**D**), and N2 (**E**) HIV-1 induced R-loop-negative chromosomal regions showing result
863 from DRIPc-seq in HIV-1-infected HeLa cells (blue, 0 hpi; yellow, 3 hpi; green, 6 hpi; red, 12 hpi; black, input
864 signals for each indicated sample) on plus (+) or minus (-) DNA strand. Magenta dotted lines represent primer
865 binding sites in qPCR following DRIP.

866

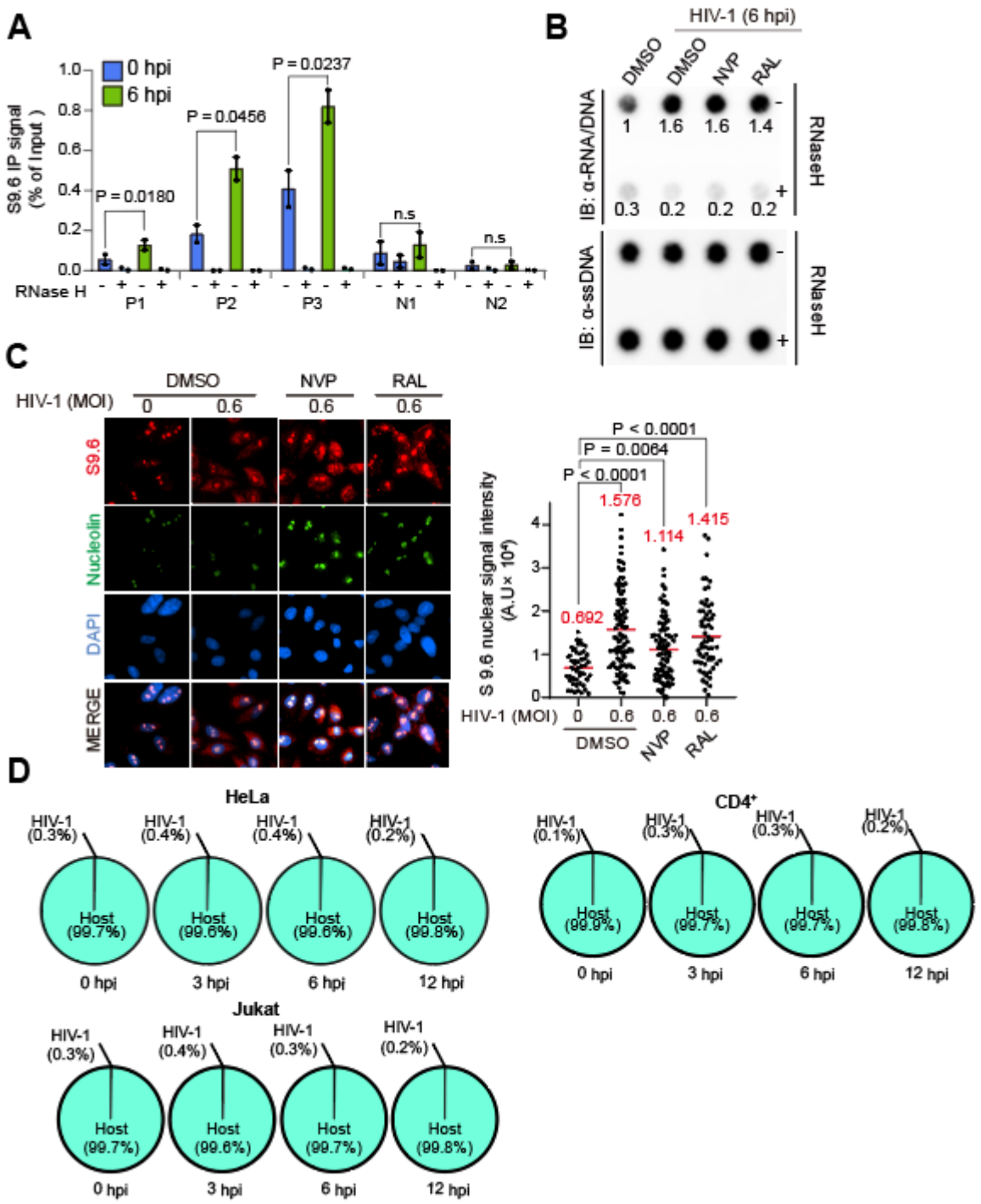

S3 Fig. Host cellular R-loop induction by HIV-1 infection is host-genome specific. (A) DRIP-qPCR using the anti-S9.6 antibody at P1, P2, P3, N1, and N2 in HIV-1-infected cells with MOI of 0.6 harvested at the indicated hpi (blue, 0 hpi; green, 6 hpi). Pre-immunoprecipitated materials were untreated (−) or treated (+) with RNase H, as indicated. Data are presented as the mean ± SEM; P-values were calculated using one-way ANOVA (n = 2).

872 (**B**) Dot blot analysis of the R-loop in gDNA extracts from HIV-1 infected HeLa cells with MOI of 0.6 harvested
873 at 6hpi. The cells were treated with DMSO, 10uM of Nevirapine (NVP), or 10uM of Raltegravir (RAL) for 24 h
874 before infection, as indicated. gDNAs were probed with anti-S9.6. gDNA extracts were incubated with or without
875 RNase H in vitro before membrane loading (anti-RNA/DNA signal). Fold-induction was normalized to the value
876 of harvested cells at 0 hpi by quantifying the dot intensity of the blots and calculating the ratios of the S9.6 signal
877 to the total amount of gDNA (anti-ssDNA signal). (**C**) Representative images of the immunofluorescence assay
878 of S9.6 nuclear signals in HIV-1 infected HeLa cells with MOI of 0.6 at 6 hpi. The cells were pre-extracted of
879 cytoplasm and co-stained with anti-S9.6 (red), anti-nucleolin antibodies (green), and DAPI (blue). The cells were
880 treated with DMSO, 10uM of Nevirapine (NVP), or 10uM of Raltegravir (RAL) for 24 h before infection, as
881 indicated. Quantification of S9.6 signal intensity per nucleus after nucleolar signal subtraction for the
882 immunofluorescence assay. The mean value for each data point is indicated by the red line. Statistical significance
883 was assessed using one-way ANOVA ($n > 51$). (**D**) Pie graphs indicating the percentage of DRIPc-seq reads aligned
884 to host cellular genome (aquamarine) or to HIV-1 viral genome (gray), out of the total consensus DRIPc-seq peaks
885 from HIV-infected HeLa cells, primary $CD4^+$ T cells and Jurkat cells.

886

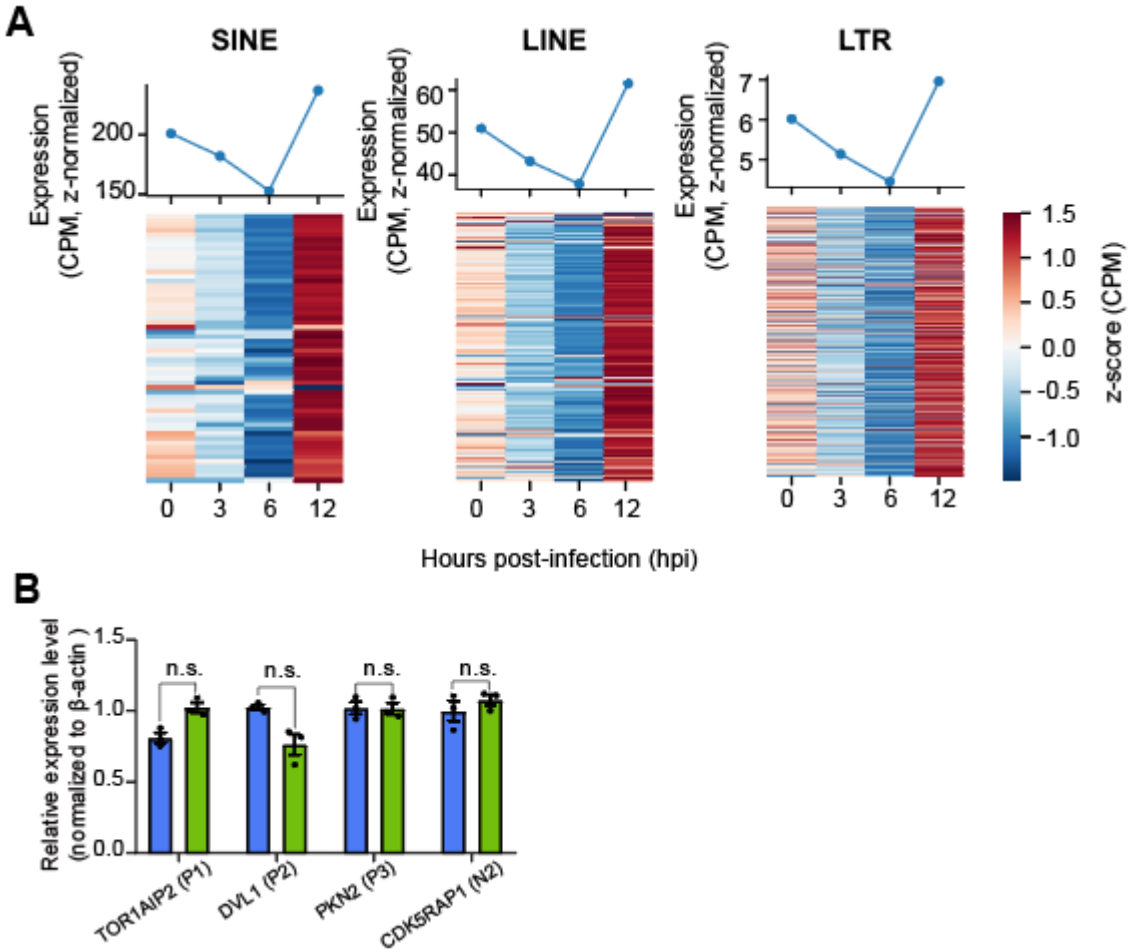

S4 Fig. R-loop induction by HIV-1 infection does not follow transcriptome changes in HeLa cells. (**A**) Line graphs and heat maps representing expression levels of indicated repetitive elements (SINE, right; LINE, middle; LTR, left) at the indicated hpi of HIV-1 in HeLa cells. Data are presented as the mean expression levels of two biologically independent experiments. (**B**) Indicated gene expression as measured by RT-qPCR in 0 or 6 hpi harvested HIV-1-infected HeLa cells. Data represent mean ± SEM, n = 3, P values were calculated according to two-tailed Student's t-test. P > 0.05; n.s, not significant.

A

Cell line	Pbcopy avg Ct	UCR1 avg Ct	ΔΔCt: 2^-(Pbcopy-UCR1)	Copy #per Genome (ΔΔCt/2)
pgR-poor	20.15	25.91	54.19	27
pgR-rich	20.12	25.63	45.57	23

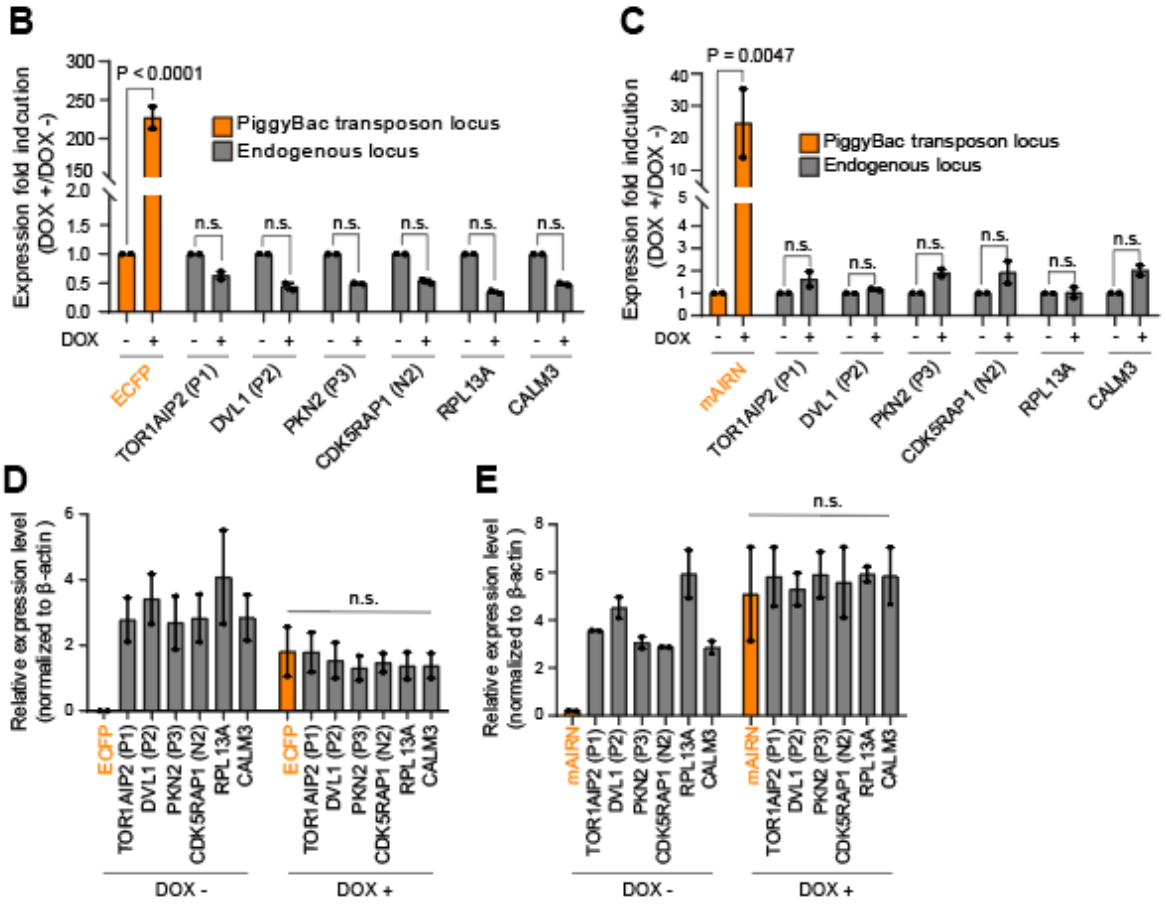

S5 Fig. Regulation of cellular R-loops by RNase H1 expression, or by transposon-transposase insertion of R-loop forming and non-R-loop forming sequences in HeLa cells. (**A**) Copy number of piggyBac transposon inserts in each cell line constructed by transfecting the transposon vector and transposase-expressing vector. (**B** and **C**) Fold induction of gene expression for the indicated genes as measured by RT-qPCR. Fold induction were calculated by dividing the gene expression level of DOX-treated (+) by that of DOX-untreated (-) in pgR-poor cells (**B**) or pgR-rich cells (**C**). Data represent mean ± SEM, n = 2, P values were calculated according to two-way ANOVA. P > 0.05; n.s, not significant. (**D** and **E**) Relative gene expression of the indicated genes as measured by RT-qPCR in DOX-treated (+) or DOX-untreated (-) pgR-poor cells (**D**) or pgR-rich cells (**E**). Data represent mean ± SEM, n = 2, P values were calculated according to two-way ANOVA. P > 0.05; n.s, not significant.

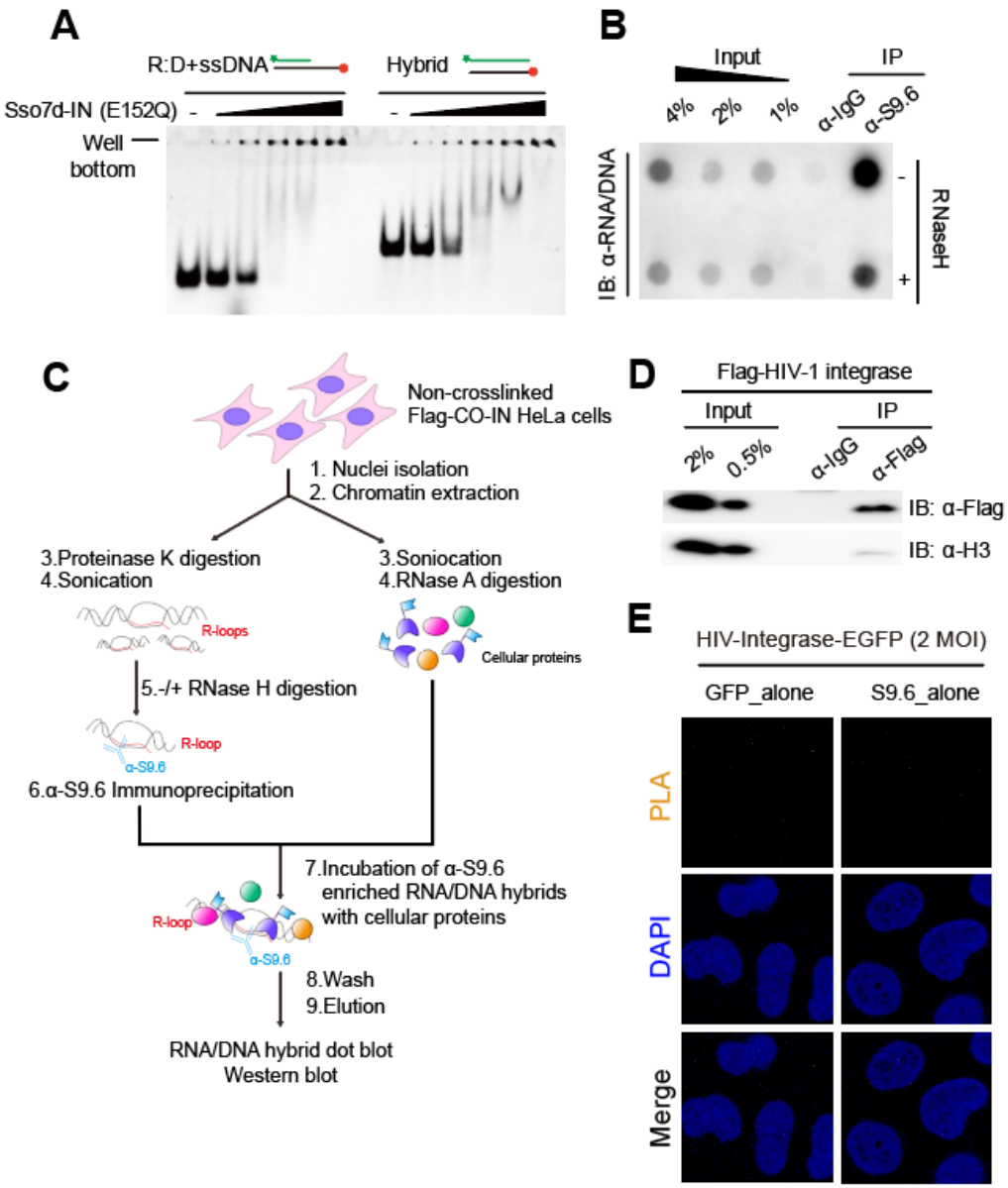

S6 Fig. HIV-1 integrase proteins directly binds to host genomic R-loops. (**A**) Representative gel images for EMSA of Sso7d-tagged HIV-1-integrase (E152Q) with different types of nucleic acids substrates (R:D+ssDNA and Hybrid). 100 nM nucleic acid substrate was incubated with Sso7d-tagged HIV-1-integrase (E152Q) at 0 nM, 20 nM, 50 nM, 100 nM, 200 nM, and 400 nM (n = 3). (**B**) Nucleic acid extracts from FLAG-HIV-1-integrase-expressing cells were immunoprecipitated using S9.6 antibody. gDNA was precipitated from the elutes of immunoprecipitation and subjected to DNA–RNA hybrid dot blotting. Where indicated, the gDNA extracts were either untreated (–) or treated (+) with RNase H after elution of immunoprecipitated materials. (**C**) Summary of the experimental design for R-loop immunoprecipitation using S9.6 antibody in FLAG-tagged HIV-1 integrase

915 protein-expressing HeLa cells with pre-immunoprecipitation in vitro RNase H treatment. (**D**) Protein extracts
916 from FLAG-HIV-1-integrase-expressing cells were immunoprecipitated using anti-FLAG antibody. Western blot
917 of FLAG immunoprecipitation was probed with anti-FLAG or anti-H3 antibodies. (**E**) Representative images of
918 the proximity-ligation assay (PLA) using single antibody (anti-GFP or anti-S9.6) in HIV-IN-EGFP virion-infected
919 HeLa cells at 6 hpi, as PLA signal negative controls. Cells were subjected to PLA (orange) and co-stained with
920 DAPI (blue) ($n > 50$).

921

HeLa				
Gene	**Chromosom**	**Position (hg38)**	**Description**	**Average DRIPc-seq signal**
RPL13A	chr19	49487608-49493057	Input (-)_0hpi	3.59
			Input (-)_3hpi	0.24
			Input (-)_6hpi	2.39
			Input (-)_12hpi	3.51
			Input (+)_0hpi	82.29
			Input (+)_3hpi	51.76
			Input (+)_6hpi	39.14
			Input (+)_12hpi	176.73
			IP_RNase H- (-)_0hpi	2.21
			IP_RNase H- (-)_3hpi	2.73
			IP_RNase H- (-)_6hpi	2.39
			IP_RNase H- (-)_12hpi	4.25
			IP_RNase H- (+)_0hpi	110.32
			IP_RNase H- (+)_3hpi	140.22
			IP_RNase H- (+)_6hpi	58.36
			IP_RNase H- (+)_12hpi	137.37
			IP_RNase H+ (-)_0hpi	0.00
			IP_RNase H+ (-)_3hpi	4.48
			IP_RNase H+ (-)_6hpi	3.74
			IP_RNase H+ (-)_12hpi	0.00
			IP_RNase H+ (+)_0hpi	1.98
			IP_RNase H+ (+)_3hpi	3.36
			IP_RNase H+ (+)_6hpi	1.60
			IP_RNase H+ (+)_12hpi	6.81
Gene	**Chromosom**	**Position (hg38)**	**Description**	**Average DRIPc-seq signal**
CALM3	chr19	46601330-46610782	Input (-)_0hpi	1.47
			Input (-)_3hpi	1.02
			Input (-)_6hpi	2.46
			Input (-)_12hpi	0.74
			Input (+)_0hpi	26.50
			Input (+)_3hpi	19.95
			Input (+)_6hpi	11.61
			Input (+)_12hpi	56.92
			IP_RNase H- (-)_0hpi	0.90
			IP_RNase H- (-)_3hpi	1.54
			IP_RNase H- (-)_6hpi	1.23
			IP_RNase H- (-)_12hpi	1.73
			IP_RNase H- (+)_0hpi	13.97
			IP_RNase H- (+)_3hpi	28.68
			IP_RNase H- (+)_6hpi	10.58
			IP_RNase H- (+)_12hpi	24.70
			IP_RNase H+ (-)_0hpi	0.71
			IP_RNase H+ (-)_3hpi	1.83
			IP_RNase H+ (-)_6hpi	2.78
			IP_RNase H+ (-)_12hpi	1.04
			IP_RNase H+ (+)_0hpi	2.12
			IP_RNase H+ (+)_3hpi	1.64
			IP_RNase H+ (+)_6hpi	2.26
			IP_RNase H+ (+)_12hpi	1.65
Gene	**Chromosom**	**Position (hg38)**	**Description**	**Average DRIPc-seq signal**
SNRPN	chr15	24823647-24978582	Input (-)_0hpi	1.46
			Input (-)_3hpi	1.27
			Input (-)_6hpi	1.34
			Input (-)_12hpi	1.76
			Input (+)_0hpi	1.21
			Input (+)_3hpi	0.81
			Input (+)_6hpi	1.25
			Input (+)_12hpi	0.41
			IP_RNase H- (-)_0hpi	0.45
			IP_RNase H- (-)_3hpi	0.47
			IP_RNase H- (-)_6hpi	0.37
			IP_RNase H- (-)_12hpi	0.05
			IP_RNase H- (+)_0hpi	0.37
			IP_RNase H- (+)_3hpi	0.24
			IP_RNase H- (+)_6hpi	0.54
			IP_RNase H- (+)_12hpi	0.07
			IP_RNase H+ (-)_0hpi	1.40
			IP_RNase H+ (-)_3hpi	0.93
			IP_RNase H+ (-)_6hpi	1.10
			IP_RNase H+ (-)_12hpi	1.31
			IP_RNase H+ (+)_0hpi	1.18
			IP_RNase H+ (+)_3hpi	1.12
			IP_RNase H+ (+)_6hpi	1.26
			IP_RNase H+ (+)_12hpi	1.10

S1 Table. Chromosomal position and DRIPc-seq signal for referenced R-loop-positive and –negative regions in HIV-1 infected HeLa cells

CD4+				
Gene	**Chromosom**	**Position (hg38)**	**Description**	**Average DRIPc-seq signal**
RPL13A	chr19	49487608-49493057	Input (-)_0hpi	2.33
			Input (-)_3hpi	1.51
			Input (-)_6hpi	2.56
			Input (-)_12hpi	0.77
			Input (+)_0hpi	2.91
			Input (+)_3hpi	1.94
			Input (+)_6hpi	2.36
			Input (+)_12hpi	2.19
			IP_RNase H- (-)_0hpi	0.00
			IP_RNase H- (-)_3hpi	3.63
			IP_RNase H- (-)_6hpi	0.00
			IP_RNase H- (-)_12hpi	0.00
			IP_RNase H- (+)_0hpi	144.19
			IP_RNase H- (+)_3hpi	77.26
			IP_RNase H- (+)_6hpi	130.86
			IP_RNase H- (+)_12hpi	190.08
			IP_RNase H+ (-)_0hpi	1.42
			IP_RNase H+ (-)_3hpi	0.00
			IP_RNase H+ (-)_6hpi	0.00
			IP_RNase H+ (-)_12hpi	0.00
			IP_RNase H+ (+)_0hpi	0.93
			IP_RNase H+ (+)_3hpi	0.00
			IP_RNase H+ (+)_6hpi	0.00
			IP_RNase H+ (+)_12hpi	2.28
Gene	**Chromosom**	**Position (hg38)**	**Description**	**Average DRIPc-seq signal**
CALM3	chr19	46601330-46610782	Input (-)_0hpi	4.58
			Input (-)_3hpi	4.64
			Input (-)_6hpi	2.96
			Input (-)_12hpi	4.04
			Input (+)_0hpi	3.62
			Input (+)_3hpi	3.65
			Input (+)_6hpi	3.40
			Input (+)_12hpi	4.11
			IP_RNase H- (-)_0hpi	0.00
			IP_RNase H- (-)_3hpi	0.00
			IP_RNase H- (-)_6hpi	0.00
			IP_RNase H- (-)_12hpi	2.70
			IP_RNase H- (+)_0hpi	108.23
			IP_RNase H- (+)_3hpi	183.80
			IP_RNase H- (+)_6hpi	87.73
			IP_RNase H- (+)_12hpi	181.80
			IP_RNase H+ (-)_0hpi	2.80
			IP_RNase H+ (-)_3hpi	0.00
			IP_RNase H+ (-)_6hpi	0.00
			IP_RNase H+ (-)_12hpi	1.94
			IP_RNase H+ (+)_0hpi	4.11
			IP_RNase H+ (+)_3hpi	1.19
			IP_RNase H+ (+)_6hpi	9.88
			IP_RNase H+ (+)_12hpi	6.17
Gene	**Chromosom**	**Position (hg38)**	**Description**	**Average DRIPc-seq signal**
SNRPN	chr15	24823647-24978582	Input (-)_0hpi	1.65
			Input (-)_3hpi	1.41
			Input (-)_6hpi	1.74
			Input (-)_12hpi	1.15
			Input (+)_0hpi	1.72
			Input (+)_3hpi	1.46
			Input (+)_6hpi	1.97
			Input (+)_12hpi	1.29
			IP_RNase H- (-)_0hpi	0.31
			IP_RNase H- (-)_3hpi	0.27
			IP_RNase H- (-)_6hpi	0.10
			IP_RNase H- (-)_12hpi	0.27
			IP_RNase H- (+)_0hpi	0.98
			IP_RNase H- (+)_3hpi	1.00
			IP_RNase H- (+)_6hpi	0.53
			IP_RNase H- (+)_12hpi	0.56
			IP_RNase H+ (-)_0hpi	0.94
			IP_RNase H+ (-)_3hpi	1.57
			IP_RNase H+ (-)_6hpi	0.00
			IP_RNase H+ (-)_12hpi	2.17
			IP_RNase H+ (+)_0hpi	1.37
			IP_RNase H+ (+)_3hpi	1.14
			IP_RNase H+ (+)_6hpi	1.42
			IP_RNase H+ (+)_12hpi	1.19

S2 Table. Chromosomal position and DRIPc-seq signal for referenced R-loop-positive and –negative regions in HIV-1 infected primary CD4^{+} T cells

Jurkat				
Gene	**Chromosom**	**Position (hg38)**	**Description**	**Average DRIPc-seq signal**
RPL13A	chr19	49487608-49493057	Input (-)_0hpi	1.46
			Input (-)_3hpi	1.92
			Input (-)_6hpi	1.92
			Input (-)_12hpi	1.58
			Input (+)_0hpi	1.40
			Input (+)_3hpi	2.02
			Input (+)_6hpi	1.15
			Input (+)_12hpi	1.54
			IP_RNase H- (-)_0hpi	0.00
			IP_RNase H- (-)_3hpi	10.17
			IP_RNase H- (-)_6hpi	9.60
			IP_RNase H- (-)_12hpi	2.64
			IP_RNase H- (+)_0hpi	404.40
			IP_RNase H- (+)_3hpi	183.88
			IP_RNase H- (+)_6hpi	486.50
			IP_RNase H- (+)_12hpi	526.25
			IP_RNase H+ (-)_0hpi	0.00
			IP_RNase H+ (-)_3hpi	3.53
			IP_RNase H+ (-)_6hpi	0.00
			IP_RNase H+ (-)_12hpi	0.00
			IP_RNase H+ (+)_0hpi	6.13
			IP_RNase H+ (+)_3hpi	0.00
			IP_RNase H+ (+)_6hpi	0.00
			IP_RNase H+ (+)_12hpi	0.00
Gene	**Chromosom**	**Position (hg38)**	**Description**	**Average DRIPc-seq signal**
CALM3	chr19	46601330-46610782	Input (-)_0hpi	2.40
			Input (-)_3hpi	2.18
			Input (-)_6hpi	2.26
			Input (-)_12hpi	2.78
			Input (+)_0hpi	2.08
			Input (+)_3hpi	2.78
			Input (+)_6hpi	1.99
			Input (+)_12hpi	2.38
			IP_RNase H- (-)_0hpi	0.00
			IP_RNase H- (-)_3hpi	11.73
			IP_RNase H- (-)_6hpi	5.58
			IP_RNase H- (-)_12hpi	5.22
			IP_RNase H- (+)_0hpi	208.25
			IP_RNase H- (+)_3hpi	182.67
			IP_RNase H- (+)_6hpi	167.98
			IP_RNase H- (+)_12hpi	220.30
			IP_RNase H+ (-)_0hpi	0.00
			IP_RNase H+ (-)_3hpi	2.04
			IP_RNase H+ (-)_6hpi	0.00
			IP_RNase H+ (-)_12hpi	4.84
			IP_RNase H+ (+)_0hpi	13.84
			IP_RNase H+ (+)_3hpi	1.62
			IP_RNase H+ (+)_6hpi	4.37
			IP_RNase H+ (+)_12hpi	3.29
Gene	**Chromosom**	**Position (hg38)**	**Description**	**Average DRIPc-seq signal**
SNRPN	chr15	24823647-24978582	Input (-)_0hpi	1.75
			Input (-)_3hpi	1.94
			Input (-)_6hpi	1.87
			Input (-)_12hpi	1.84
			Input (+)_0hpi	1.86
			Input (+)_3hpi	1.89
			Input (+)_6hpi	1.81
			Input (+)_12hpi	1.73
			IP_RNase H- (-)_0hpi	0.12
			IP_RNase H- (-)_3hpi	0.00
			IP_RNase H- (-)_6hpi	0.17
			IP_RNase H- (-)_12hpi	0.00
			IP_RNase H- (+)_0hpi	2.43
			IP_RNase H- (+)_3hpi	2.19
			IP_RNase H- (+)_6hpi	2.23
			IP_RNase H- (+)_12hpi	2.36
			IP_RNase H+ (-)_0hpi	2.58
			IP_RNase H+ (-)_3hpi	3.46
			IP_RNase H+ (-)_6hpi	1.62
			IP_RNase H+ (-)_12hpi	1.87
			IP_RNase H+ (+)_0hpi	1.78
			IP_RNase H+ (+)_3hpi	2.38
			IP_RNase H+ (+)_6hpi	1.06
			IP_RNase H+ (+)_12hpi	1.43

S3 Table. Chromosomal position and DRIPc-seq signal for referenced R-loop-positive and –negative regions in HIV-1 infected Jurkat cells

	gene_symbol	0hpi	3hpi	6hpi	12hpi	48hpi
P1	TOR1AIP2	1	1.163832	1.247899	1.024926	0.619497
P2	DVL1	1	0.781593	0.571348	0.901502	0.270459
P3	PKN2	1	1.280974	1.891552	1.31842	1.515107
N1	N/A	N/A	N/A	N/A	N/A	N/A
N2	CDK5RAP1	1	0.73977	0.775	1.143662	0.472377

S4 Table. RNA-seq analysis of relative gene expression levels of P1-3 and N1,2 R-loop regions

935

936 **S5 Table. Oligonucleotides used for DRIPc-seq library construction**

Oligonucleotides	Sequence 5' to 3'	Remark
PCR primer 1.0 P5	AATGATACGGCGACCACCGAGATCTACACTCTTTCCCTACACGA	amplification primer
PCR primer 2.0 P7	CAAGCAGAAGACGGCATACGAGAT	amplification primer
Index Adapter 1	GATCGGAAGAGCACACGTCTGAACTCCAGTCACATCACGATCTCGTATGCCGTCTTCTGCTTG	HeLa 0hpi Input replicate 1
Index Adapter 2	GATCGGAAGAGCACACGTCTGAACTCCAGTCACCGATGTATCTCGTATGCCGTCTTCTGCTTG	HeLa 3hpi Input replicate 1
Index Adapter 3	GATCGGAAGAGCACACGTCTGAACTCCAGTCACTTAGGCATCTCGTATGCCGTCTTCTGCTTG	HeLa 6hpi Input replicate 1
Index Adapter 4	GATCGGAAGAGCACACGTCTGAACTCCAGTCACTGACCAATCTCGTATGCCGTCTTCTGCTTG	HeLa 12hpi Input replicate 1
Index Adapter 5	GATCGGAAGAGCACACGTCTGAACTCCAGTCACACAGTGATCTCGTATGCCGTCTTCTGCTTG	HeLa 0hpi RNH-IP replicate 1
Index Adapter 6	GATCGGAAGAGCACACGTCTGAACTCCAGTCACGCCAATATCTCGTATGCCGTCTTCTGCTTG	HeLa 3hpi RNH-IP replicate 1
Index Adapter 7	GATCGGAAGAGCACACGTCTGAACTCCAGTCACCAGATCATCTCGTATGCCGTCTTCTGCTTG	HeLa 6hpi RNH-IP replicate 1
Index Adapter 8	GATCGGAAGAGCACACGTCTGAACTCCAGTCACACTTGAATCTCGTATGCCGTCTTCTGCTTG	HeLa 12hpi RNH-IP replicate 1
Index Adapter 9	GATCGGAAGAGCACACGTCTGAACTCCAGTCACGATCAGATCTCGTATGCCGTCTTCTGCTTG	HeLa 0hpi RNH+IP replicate 1
Index Adapter 10	GATCGGAAGAGCACACGTCTGAACTCCAGTCACTAGCTTATCTCGTATGCCGTCTTCTGCTTG	HeLa 3hpi RNH+IP replicate 1
Index Adapter 11	GATCGGAAGAGCACACGTCTGAACTCCAGTCACGGCTACATCTCGTATGCCGTCTTCTGCTTG	HeLa 6hpi RNH+IP replicate 1
Index Adapter 12	GATCGGAAGAGCACACGTCTGAACTCCAGTCACCTTGTAATCTCGTATGCCGTCTTCTGCTTG	HeLa 12hpi RNH+IP replicate 1
Index Adapter 28	GATCGGAAGAGCACACGTCTGAACTCCAGTCACCAAAAGATCTCGTATGCCGTCTTCTGCTTG	HeLa 0hpi Input replicate 2
Index Adapter 29	GATCGGAAGAGCACACGTCTGAACTCCAGTCACCAACTAATCTCGTATGCCGTCTTCTGCTTG	HeLa 3hpi Input replicate 2
Index Adapter 30	GATCGGAAGAGCACACGTCTGAACTCCAGTCACCACCGGATCTCGTATGCCGTCTTCTGCTTG	HeLa 6hpi Input replicate 2
Index Adapter 31	GATCGGAAGAGCACACGTCTGAACTCCAGTCACCACGATATCTCGTATGCCGTCTTCTGCTTG	HeLa 12hpi Input replicate 2
Index Adapter 32	GATCGGAAGAGCACACGTCTGAACTCCAGTCACCACTCAATCTCGTATGCCGTCTTCTGCTTG	HeLa 0hpi RNH-IP replicate 2
Index Adapter 33	GATCGGAAGAGCACACGTCTGAACTCCAGTCACCAGGCGATCTCGTATGCCGTCTTCTGCTTG	HeLa 3hpi RNH-IP replicate 2
Index Adapter 34	GATCGGAAGAGCACACGTCTGAACTCCAGTCACCATGGCATCTCGTATGCCGTCTTCTGCTTG	HeLa 6hpi RNH-IP replicate 2
Index Adapter 35	GATCGGAAGAGCACACGTCTGAACTCCAGTCACCATTTTATCTCGTATGCCGTCTTCTGCTTG	HeLa 12hpi RNH-IP replicate 2
Index Adapter 36	GATCGGAAGAGCACACGTCTGAACTCCAGTCACCCAACAATCTCGTATGCCGTCTTCTGCTTG	HeLa 0hpi RNH+IP replicate 2
Index Adapter 37	GATCGGAAGAGCACACGTCTGAACTCCAGTCACCGGAATATCTCGTATGCCGTCTTCTGCTTG	HeLa 3hpi RNH+IP replicate 2
Index Adapter 38	GATCGGAAGAGCACACGTCTGAACTCCAGTCACCTAGCTATCTCGTATGCCGTCTTCTGCTTG	HeLa 6hpi RNH+IP replicate 2
Index Adapter 39	GATCGGAAGAGCACACGTCTGAACTCCAGTCACCTATACATCTCGTATGCCGTCTTCTGCTTG	HeLa 12hpi RNH+IP replicate 2

Oligonucleotides	Sequence 5' to 3'
P1 Fwd	TTATAAGTCAGCCTCCAGGATCAA
P1 Rev	TTCAGGTCTAGGCAGTCTGA
P2 Fwd	GGA CAG ATG ACA GGG TCG C
P2 Rev	ATG AGG AAG ACC CCC TCG G
P3 Fwd	CTCTGTGTAACGCTGGTGCT
P3 Rev	ACACGCTTCTGACCACTAAGG
N1 Fwd	TTG GCC CTA CTG AAT GAT TGG T
N1 Rev	TTA AGG CAT GCT CAG GCG A
N2 Fwd	TGA GAT TTC AGG TTC CAT GAT TTG
N2 Rev	TGC TCA GTG TTC TAA TTT CCC TGT
β-actin Fwd	AGAGCTACGAGCTGCCTGAC
β-actin Rev	AGCACTGTGTTGGCGTACAG
SH49 (ECFP Fwd)	TGGTTTGTCCAAACTCATCAA
SH40 (mAlRN Fwd)	CGAGAGAGGCTAAGGGTGAA
SH21 (ECFP/mAlRN Rev)	ACATGGTCCTGCTGGAGTTC
RT-qPCR P1 (TOR1AIP2) Fwd	CCTTGGTCTTTCCCACTTGAGTG
RT-qPCR P1 (TOR1AIP2) Rev	GCAGGGTTAAAACCAGCTACTCG
RT-qPCR P2 (DVL1) Fwd	GCATAACCGACTCCACCATGTC
RT-qPCR P2 (DVL1) Rev	GATGGAGCCAATGTAGATGCCG
RT-qPCR P3 (PKN2) Fwd	GCATCACCAACACTAAGTCCACG
RT-qPCR P3 (PKN2) Rev	GCTTTTGACCGTCCAGGGACAT
RT-qPCR N2 (CDK5RAP1) Fwd	AGAGTGGAAGCAGCCGTGTGTT
RT-qPCR N2 (CDK5RAP1) Rev	GATCTTCCTCCGTCTCACCACA

S6 Table. Primers used for qPCR

Oligonucleotides	Sequence 5' to 3'	Remark
AE5316	TGTGACTCTGGTAACTAGAGATCCCTC	First round LTR primer
AE6380	TAGTCCCTTAAGCGGAG-NH2	replicate 1 5dpi Linker short / replicate 1 pgR-poor DOX- Linker short / CD4+ donor 1 Linker short
AE6381	GTAATACGACTCACTATAGGGCCTCCGCTTAAGGGAC	replicate 1 5dpi Linker long / replicate 1 pgR-poor DOX- Linker long / CD4+ donor 1 Linker long
AE6382	CAAGCAGAAGACGGCATACGAGATCGGTCTCGGCATTCCTGCTGAACCGCTCTTCCGATCTGTAATACGACTCACTATAGGGC	replicate 1 5dpi Linker primer / replicate 1 pgR-poor DOX- Linker primer / CD4+ donor 1 Linker primer
AE6404	AATGATACGGCGACCACCGAGATCTACACTCTTTCCCTACACGACGCTCTTCCGATCTCGATGTGAGATCCCTCAGACCCTTTTAGTCAG	replicate 1 5dpi Second round LTR primer / replicate 1 pgR-poor DOX- Second round LTR primer / CD4+ donor 1 Second round LTR primer
AE6380	TAGTCCCTTAAGCGGAG-NH2	replicate 2 5dpi Linker short / replicate 2 pgR-poor DOX+ Linker short
AE6381	GTAATACGACTCACTATAGGGCCTCCGCTTAAGGGAC	replicate 2 5dpi Linker long / replicate 2 pgR-poor DOX+ Linker long
AE6382	CAAGCAGAAGACGGCATACGAGATCGGTCTCGGCATTCCTGCTGAACCGCTCTTCCGATCTGTAATACGACTCACTATAGGGC	replicate 2 5dpi Linker primer / replicate 2 pgR-poor DOX+ Linker prime
AE6404-1	AATGATACGGCGACCACCGAGATCTACACTCTTTCCCTACACGACGCTCTTCCGATCTTTAGGCGAGATCCCTCAGACCCTTTTAGTCAG	replicate 2 5dpi Second round LTR primer / replicate 2 pgR-poor DOX+ Second round LTR primer
AE6386	TACTATGACGGTGACGC-NH2	replicate 1 pgR-rich DOX- Linker short / CD4+ donor 2 Linker short
AE6387	GAGAATCCATGAGTATGCTCACGCGTCACCGTCATAG	replicate 1 pgR-rich DOX- Linker long / CD4+ donor 2 Linker long
AE6388	CAAGCAGAAGACGGCATACGAGATCGGTCTCGGCATTCCTGCTGAACCGCTCTTCCGATCTGAGAATCCATGAGTATGCTCAC	replicate 1 pgR-rich DOX- Linker primer / CD4+ donor 2 Linker primer
AE6406	AATGATACGGCGACCACCGAGATCTACACTCTTTCCCTACACGACGCTCTTCCGATCTACAGTGGAGATCCCTCAGACCCTTTTAGTCAG	replicate 1 pgR-rich DOX- Second round LTR primer / CD4+ donor 2 Second round LTR primer
AE6456	TAGACTGACGCAGTCTG-NH2	replicate 1 pgR-poor DOX+ Linker short
AE6457	GACGTACATACTGATCGCATAGCAGACTGCGTCAGTC	replicate 1 pgR-poor DOX+ Linker long
AE6458	CAAGCAGAAGACGGCATACGAGATCGGTCTCGGCATTCCTGCTGAACCGCTCTTCCGATCTGACGTACATACTGATCGCATAG	replicate 1 pgR-poor DOX+ Linker primer
AE6405	AATGATACGGCGACCACCGAGATCTACACTCTTTCCCTACACGACGCTCTTCCGATCTTGACCAGAGATCCCTCAGACCCTTTTAGTCAG	replicate 1 pgR-poor DOX+ Second round LTR primer
AE6386	TACTATGACGGTGACGC-NH2	replicate 2 pgR-rich DOX+ Linker short
AE6387	GAGAATCCATGAGTATGCTCACGCGTCACCGTCATAG	replicate 2 pgR-rich DOX+ Linker long
AE6388	CAAGCAGAAGACGGCATACGAGATCGGTCTCGGCATTCCTGCTGAACCGCTCTTCCGATCTGAGAATCCATGAGTATGCTCAC	replicate 2 pgR-rich DOX+ Linker primer
AE6406-1	AATGATACGGCGACCACCGAGATCTACACTCTTTCCCTACACGACGCTCTTCCGATCTGCCAATGAGATCCCTCAGACCCTTTTAGTCAG	replicate 2 pgR-rich DOX+ Second round LTR primer
AE6456	TAGACTGACGCAGTCTG-NH2	replicate 3 pgR-rich DOX- Linker short
AE6457	GACGTACATACTGATCGCATAGCAGACTGCGTCAGTC	replicate 3 pgR-rich DOX- Linker long
AE6458	CAAGCAGAAGACGGCATACGAGATCGGTCTCGGCATTCCTGCTGAACCGCTCTTCCGATCTGACGTACATACTGATCGCATAG	replicate 3 pgR-rich DOX- Linker primer
AE6411	AATGATACGGCGACCACCGAGATCTACACTCTTTCCCTACACGACGCTCTTCCGATCTAGTTCCGAGATCCCTCAGACCCTTTTAGTCAG	replicate 3 pgR-rich DOX- Second round LTR primer
AE6392	TACTGAGACGTCGATGC-NH2	replicate 1 RNH_mut 5dpi Linker short / replicate 2 RNH_mut 5dpi Linker short
AE6393	GATCATGCGAGATACATCTCAGGCATCGACGTCTCAG	replicate 1 RNH_mut 5dpi Linker long / replicate 2 RNH_mut 5dpi Linker long
AE6394	CAAGCAGAAGACGGCATACGAGATCGGTCTCGGCATTCCTGCTGAACCGCTCTTCCGATCTGATCATGCGAGATACATCTCAG	replicate 1 RNH_mut 5dpi Linker primer / replicate 2 RNH_mut 5dpi Linker primer
AE6493	AATGATACGGCGACCACCGAGATCTACACTCTTTCCCTACACGACGCTCTTCCGATCTGGCTACGAGATCCCTCAGACCCTTTTAGTCAG	replicate 1 RNH_mut 5dpi Second round LTR primer
AE6493-1	AATGATACGGCGACCACCGAGATCTACACTCTTTCCCTACACGACGCTCTTCCGATCTACTTGAGAGATCCCTCAGACCCTTTTAGTCAG	replicate 2 RNH_mut 5dpi Second round LTR primer
AE6462	TAGTAGTCACGAGCGTC-NH2	replicate 1 RNH_wt 5dpi Linker short / replicate 2 RNH_wt 5dpi Linker short
AE6463	CAGTTAGACTACACGTTAGACGGACGCTCGTGACTAC	replicate 1 RNH_wt 5dpi Linker long / replicate 2 RNH_wt 5dpi Linker long
AE6464	CAAGCAGAAGACGGCATACGAGATCGGTCTCGGCATTCCTGCTGAACCGCTCTTCCGATCTCAGTTAGACTACACGTTAGACG	replicate 1 RNH_wt 5dpi Linker primer / replicate 2 RNH_wt 5dpi Linker primer
AE6492	AATGATACGGCGACCACCGAGATCTACACTCTTTCCCTACACGACGCTCTTCCGATCTTAGCTTGAGATCCCTCAGACCCTTTTAGTCAG	replicate 1 RNH_wt 5dpi Second round LTR primer
AE6497	AATGATACGGCGACCACCGAGATCTACACTCTTTCCCTACACGACGCTCTTCCGATCTATCACGGAGATCCCTCAGACCCTTTTAGTCAG	replicate 2 RNH_wt 5dpi Second round LTR primer

S7 Table. Oligonucleotides used for HIV-1 integration site sequencing library construct

Oligonucleotides	Sequence 5' to 3'	Remark
R-loop oligo1*	5'-[Cy3]-GCC AGG GAC GAG GTG AAC CTG CAG GTG GGC GGC TAC TAC TTA GAT GTC ATC CGA GGC TTA TTG GTA GAA TTC GGC AGC GTC ATG C GA CGG C-3'	R-loop, R:D+ssDNA, ssDNA
R-loop oligo2*	5'-GCC GTC GCA TGA CGC TGC CGA ATT CTA CCA CGC GAT TCA TAC CTG TCG TGC CAG CTG CTT TGC CCA CCT GCA GGT TCA CCT CGT CCC TGG C-3'	R-loop, dsDNA
R-loop RNA	5'-[Cy5]-GCA GCU GGC ACG ACA GGU AUG AAU C-3'	R-loop, R:D+ssDNA, ssRNA
Homoduplex	5'-[Cy3]-GCC AGG GAC GAG GTG AAC CTG CAG GTG GGC AAA GCA GCT GGC ACG ACA GGT ATG AAT CGC GTG GTA GAA TTC GGC AGC GTC ATG CGA CGG C-3'	dsDNA
Hybrid DNA	5'-CCC ATA CCG TAT AAC CAT TTG GCT GTC CAA GCT CCG GGT-3'	Hybrid
Hybrid RNA	5'-[Cy5]-ACC CGG AGC UUG GAC AGC CAA AUG GUU AUA CGG UAU GGG-3'	Hybrid
oligo 5	5′GCAGTAGCATGACGCTGCTGAATTCTACCACGCTATGCT CTCGTCTAGGTTCACTCCGT CCCTGCGATTCATACCTGTCGTGCCAGCTGC	R:D+ssDNA

S8 Table. Oligonucleotides used for electrophoretic mobility shift assay substrate preparation

Data	Accession Number/ Website
Jurkat integration site	SRR12322252
TSA-seq_SPAD	SRR3538917, SRR3538918, SRR3538919, SRR3538920
SPIN (Spatial Position Inference of the Nuclear genome) annotation of speckle	https://github.com/ma-compbio/SPIN
LADs	GSE22428

S9 Table. Accession numbers and data sources.

946 # References

947 1. W. E. Johnson, Origins and evolutionary consequences of ancient endogenous retroviruses.
948 *Nat Rev Microbiol* **17**, 355-370 (2019).
949 2. M. Lusic, R. F. Siliciano, Nuclear landscape of HIV-1 infection and integration. *Nat Rev*
950 *Microbiol* **15**, 69-82 (2017).
951 3. H. C. Chen, J. P. Martinez, E. Zorita, A. Meyerhans, G. J. Filion, Position effects influence HIV
952 latency reversal. *Nat Struct Mol Biol* **24**, 47-54 (2017).
953 4. K. B. Einkauf *et al.*, Parallel analysis of transcription, integration, and sequence of single HIV-
954 1 proviruses. *Cell* **185**, 266-282 e215 (2022).
955 5. C. Jiang *et al.*, Distinct viral reservoirs in individuals with spontaneous control of HIV-1.
956 *Nature* **585**, 261-267 (2020).
957 6. A. R. Schroder *et al.*, HIV-1 integration in the human genome favors active genes and local
958 hotspots. *Cell* **110**, 521-529 (2002).
959 7. V. Achuthan *et al.*, Capsid-CPSF6 Interaction Licenses Nuclear HIV-1 Trafficking to Sites of
960 Viral DNA Integration. *Cell Host Microbe* **24**, 392-404 e398 (2018).
961 8. A. Ciuffi *et al.*, A role for LEDGF/p75 in targeting HIV DNA integration. *Nat Med* **11**, 1287-
962 1289 (2005).
963 9. G. A. Sowd *et al.*, A critical role for alternative polyadenylation factor CPSF6 in targeting
964 HIV-1 integration to transcriptionally active chromatin. *Proc Natl Acad Sci U S A* **113**, E1054-
965 1063 (2016).
966 10. B. Lucic *et al.*, Spatially clustered loci with multiple enhancers are frequent targets of HIV-1
967 integration. *Nat Commun* **10**, 4059 (2019).
968 11. B. Marini *et al.*, Nuclear architecture dictates HIV-1 integration site selection. *Nature* **521**,
969 227-231 (2015).
970 12. M. Kvaratskhelia, A. Sharma, R. C. Larue, E. Serrao, A. Engelman, Molecular mechanisms of
971 retroviral integration site selection. *Nucleic Acids Res* **42**, 10209-10225 (2014).
972 13. P. Cherepanov *et al.*, HIV-1 integrase forms stable tetramers and associates with LEDGF/p75
973 protein in human cells. *J Biol Chem* **278**, 372-381 (2003).
974 14. J. M. Coffin *et al.*, Integration in oncogenes plays only a minor role in determining the in
975 vivo distribution of HIV integration sites before or during suppressive antiretroviral therapy.
976 *PLoS Pathog* **17**, e1009141 (2021).
977 15. C. Niehrs, B. Luke, Regulatory R-loops as facilitators of gene expression and genome stability.
978 *Nat Rev Mol Cell Biol* **21**, 167-178 (2020).
979 16. E. Petermann, L. Lan, L. Zou, Sources, resolution and physiological relevance of R-loops and
980 RNA-DNA hybrids. *Nat Rev Mol Cell Biol* **23**, 521-540 (2022).
981 17. S. Hamperl, M. J. Bocek, J. C. Saldivar, T. Swigut, K. A. Cimprich, Transcription-Replication

982 Conflict Orientation Modulates R-Loop Levels and Activates Distinct DNA Damage
983 Responses. *Cell* **170**, 774-786 e719 (2017).
984 18. P. A. Ginno, P. L. Lott, H. C. Christensen, I. Korf, F. Chedin, R-loop formation is a distinctive
985 characteristic of unmethylated human CpG island promoters. *Mol Cell* **45**, 814-825 (2012).
986 19. Y. W. Lim, L. A. Sanz, X. Xu, S. R. Hartono, F. Chedin, Genome-wide DNA hypomethylation
987 and RNA:DNA hybrid accumulation in Aicardi-Goutieres syndrome. *Elife* **4**, (2015).
988 20. R. Arora *et al.*, RNaseH1 regulates TERRA-telomeric DNA hybrids and telomere maintenance
989 in ALT tumour cells. *Nat Commun* **5**, 5220 (2014).
990 21. T. Garcia-Muse, A. Aguilera, R Loops: From Physiological to Pathological Roles. *Cell* **179**,
991 604-618 (2019).
992 22. L. A. Sanz *et al.*, Prevalent, Dynamic, and Conserved R-Loop Structures Associate with Specific
993 Epigenomic Signatures in Mammals. *Mol Cell* **63**, 167-178 (2016).
994 23. F. Chedin, Nascent Connections: R-Loops and Chromatin Patterning. *Trends Genet* **32**, 828-
995 838 (2016).
996 24. C. Y. Lee *et al.*, R-loop induced G-quadruplex in non-template promotes transcription by
997 successive R-loop formation. *Nat Commun* **11**, 3392 (2020).
998 25. H. O. Ajoge *et al.*, G-Quadruplex DNA and Other Non-Canonical B-Form DNA Motifs
999 Influence Productive and Latent HIV-1 Integration and Reactivation Potential. *Viruses* **14**,
1000 (2022).
1001 26. F. Chedin, C. J. Benham, Emerging roles for R-loop structures in the management of
1002 topological stress. *J Biol Chem* **295**, 4684-4695 (2020).
1003 27. I. K. Jozwik *et al.*, B-to-A transition in target DNA during retroviral integration. *Nucleic Acids*
1004 *Res* **50**, 8898-8918 (2022).
1005 28. A. Ballandras-Colas *et al.*, Multivalent interactions essential for lentiviral integrase function.
1006 *Nat Commun* **13**, 2416 (2022).
1007 29. L. A. Sanz, F. Chedin, High-resolution, strand-specific R-loop mapping via S9.6-based DNA-
1008 RNA immunoprecipitation and high-throughput sequencing. *Nat Protoc* **14**, 1734-1755
1009 (2019).
1010 30. R. B. Jones *et al.*, LINE-1 retrotransposable element DNA accumulates in HIV-1-infected cells.
1011 *J Virol* **87**, 13307-13320 (2013).
1012 31. S. Srinivasachar Badarinarayan *et al.*, HIV-1 infection activates endogenous retroviral
1013 promoters regulating antiviral gene expression. *Nucleic Acids Res* **48**, 10890-10908 (2020).
1014 32. P. Lesbats, A. N. Engelman, P. Cherepanov, Retroviral DNA Integration. *Chem Rev* **116**, 12730-
1015 12757 (2016).
1016 33. A. Brussel, P. Sonigo, Analysis of early human immunodeficiency virus type 1 DNA synthesis
1017 by use of a new sensitive assay for quantifying integrated provirus. *J Virol* **77**, 10119-10124
1018 (2003).
1019 34. A. Albanese, D. Arosio, M. Terreni, A. Cereseto, HIV-1 pre-integration complexes selectively

1020 target decondensed chromatin in the nuclear periphery. *PLoS One* **3**, e2413 (2008).
1021 35. A. Dharan, N. Bachmann, S. Talley, V. Zwikelmaier, E. M. Campbell, Nuclear pore blockade
1022 reveals that HIV-1 completes reverse transcription and uncoating in the nucleus. *Nat*
1023 *Microbiol* **5**, 1088-1095 (2020).
1024 36. P. A. Ginno, Y. W. Lim, P. L. Lott, I. Korf, F. Chedin, GC skew at the 5' and 3' ends of human
1025 genes links R-loop formation to epigenetic regulation and transcription termination.
1026 *Genome Res* **23**, 1590-1600 (2013).
1027 37. J. J. Kessl *et al.*, HIV-1 Integrase Binds the Viral RNA Genome and Is Essential during Virion
1028 Morphogenesis. *Cell* **166**, 1257-1268 e1212 (2016).
1029 38. D. C. van Gent, Y. Elgersma, M. W. Bolk, C. Vink, R. H. Plasterk, DNA binding properties of
1030 the integrase proteins of human immunodeficiency viruses types 1 and 2. *Nucleic Acids Res*
1031 **19**, 3821-3827 (1991).
1032 39. A. Cristini, M. Groh, M. S. Kristiansen, N. Gromak, RNA/DNA Hybrid Interactome Identifies
1033 DXH9 as a Molecular Player in Transcriptional Termination and R-Loop-Associated DNA
1034 Damage. *Cell Rep* **23**, 1891-1905 (2018).
1035 40. T. Mosler *et al.*, R-loop proximity proteomics identifies a role of DDX41 in transcription-
1036 associated genomic instability. *Nat Commun* **12**, 7314 (2021).
1037 41. R. Schrijvers *et al.*, LEDGF/p75-independent HIV-1 replication demonstrates a role for HRP-
1038 2 and remains sensitive to inhibition by LEDGINs. *PLoS Pathog* **8**, e1002558 (2012).
1039 42. P. C. Stirling, P. Hieter, Canonical DNA Repair Pathways Influence R-Loop-Driven Genome
1040 Instability. *J Mol Biol* **429**, 3132-3138 (2017).
1041 43. M. L. Garcia-Rubio *et al.*, The Fanconi Anemia Pathway Protects Genome Integrity from R-
1042 loops. *PLoS Genet* **11**, e1005674 (2015).
1043 44. M. Giannini *et al.*, TDP-43 mutations link Amyotrophic Lateral Sclerosis with R-loop
1044 homeostasis and R loop-mediated DNA damage. *PLoS Genet* **16**, e1009260 (2020).
1045 45. S. Fu *et al.*, HIV-1 exploits the Fanconi anemia pathway for viral DNA integration. *Cell Rep*
1046 **39**, 110840 (2022).
1047 46. D. Li, A. Lopez, C. Sandoval, R. Nichols Doyle, O. I. Fregoso, HIV Vpr Modulates the Host
1048 DNA Damage Response at Two Independent Steps to Damage DNA and Repress Double-
1049 Strand DNA Break Repair. *mBio* **11**, (2020).
1050 47. H. Bauby *et al.*, HIV-1 Vpr Induces Widespread Transcriptomic Changes in CD4(+) T Cells
1051 Early Postinfection. *mBio* **12**, e0136921 (2021).
1052 48. K. Stopak, C. de Noronha, W. Yonemoto, W. C. Greene, HIV-1 Vif blocks the antiviral activity
1053 of APOBEC3G by impairing both its translation and intracellular stability. *Mol Cell* **12**, 591-
1054 601 (2003).
1055 49. D. Kmiec, F. Kirchhoff, Antiviral factors and their counteraction by HIV-1: many uncovered
1056 and more to be discovered. *J Mol Cell Biol*, (2024).
1057 50. J. L. McCann *et al.*, R-loop homeostasis and cancer mutagenesis promoted by the DNA

1058 cytosine deaminase APOBEC3B. 2021.2008.2030.458235 (2021).
1059 51. S. A. Yukl *et al.*, HIV latency in isolated patient CD4(+) T cells may be due to blocks in HIV
1060 transcriptional elongation, completion, and splicing. *Sci Transl Med* **10**, (2018).
1061 52. D. O. Passos *et al.*, Cryo-EM structures and atomic model of the HIV-1 strand transfer
1062 complex intasome. *Science* **355**, 89-92 (2017).
1063 53. H. D. Nguyen *et al.*, Functions of Replication Protein A as a Sensor of R Loops and a
1064 Regulator of RNaseH1. *Mol Cell* **65**, 832-847 e834 (2017).
1065 54. S. Andrews. (2010).
1066 55. F. J. Felix Krueger, Phil Ewels, Ebrahim Afyounian, & Benjamin Schuster-Boeckler,
1067 FelixKrueger/TrimGalore: v0.6.7 - DOI via Zenodo (0.6.7). Zenodo. (2021).
1068 56. M. Martin, Cutadapt removes adapter sequences from high-throughput sequencing reads.
1069 *2011* **17**, 3 %J EMBnet.journal (2011).
1070 57. H. Li, R. Durbin, Fast and accurate short read alignment with Burrows-Wheeler transform.
1071 *Bioinformatics* **25**, 1754-1760 (2009).
1072 58. Y. Zhang *et al.*, Model-based analysis of ChIP-Seq (MACS). *Genome Biol* **9**, R137 (2008).
1073 59. A. R. Quinlan, I. M. Hall, BEDTools: a flexible suite of utilities for comparing genomic features.
1074 *Bioinformatics* **26**, 841-842 (2010).
1075 60. W. Li *et al.*, CPSF6-Dependent Targeting of Speckle-Associated Domains Distinguishes
1076 Primate from Nonprimate Lentiviral Integration. *mBio* **11**, (2020).
1077 61. H. M. Amemiya, A. Kundaje, A. P. Boyle, The ENCODE Blacklist: Identification of Problematic
1078 Regions of the Genome. *Sci Rep* **9**, 9354 (2019).
1079 62. A. Frankish *et al.*, Gencode 2021. *Nucleic Acids Res* **49**, D916-D923 (2021).
1080 63. A. Dobin *et al.*, STAR: ultrafast universal RNA-seq aligner. *Bioinformatics* **29**, 15-21 (2013).
1081 64. Y. Jin, O. H. Tam, E. Paniagua, M. Hammell, TEtranscripts: a package for including
1082 transposable elements in differential expression analysis of RNA-seq datasets. *Bioinformatics*
1083 **31**, 3593-3599 (2015).

1084